AGU PUBLICATIONS

Geochemistry, Geophysics, Geosystems

RESEARCH ARTICLE
10.1002/2015GC005999

Key Points:
- CH_4 concentrations were consistently above atmospheric equilibrium
- Most parameters showed no pronounced seasonal variation
- The ^{13}C-DIC data indicate that part of the CO_2 involved in chemical weathering is geogenic

Supporting Information:
- Supporting Information S1
- Data Set S1
- Data Set S2

Correspondence to:
C. M. Balagizi,
balagizi.charles@gmail.com

Citation:
Balagizi, C. M., F. Darchambeau, S. Bouillon, M. M. Yalire, T. Lambert, and A. V. Borges (2015), River geochemistry, chemical weathering, and atmospheric CO_2 consumption rates in the Virunga Volcanic Province (East Africa), *Geochem. Geophys. Geosyst.*, *16*, doi:10.1002/2015GC005999.

Received 9 JUL 2015
Accepted 12 JUL 2015
Accepted article online 16 JUL 2015

River geochemistry, chemical weathering, and atmospheric CO_2 consumption rates in the Virunga Volcanic Province (East Africa)

Charles M. Balagizi[1,2,3], François Darchambeau[2], Steven Bouillon[4], Mathieu M. Yalire[1], Thibault Lambert[2], and Alberto V. Borges[2]

[1]Geochemistry and Environmental Department, Goma Volcano Observatory, Goma, RD Congo, [2]Chemical Oceanography Unit, Université de Liège, Liège, Belgium, [3]Department of Environmental, Biological and Pharmaceutical Sciences and Technologies, Second University of Naples, Caserta, Italy, [4]Department of Earth and Environmental Sciences, Katholieke Universiteit Leuven, Leuven-Heverlee, Belgium

Abstract We report a water chemistry data set from 13 rivers of the Virunga Volcanic Province (VVP) (Democratic Republic of Congo), sampled between December 2010 and February 2013. Most parameters showed no pronounced seasonal variation, whereas their spatial variation suggests a strong control by lithology, soil type, slope, and vegetation. High total suspended matter (289–1467 mg L^{-1}) was recorded in rivers in the Lake Kivu catchment, indicating high soil erodibility, partly as a consequence of deforestation and farming activities. Dissolved and particulate organic carbon (DOC and POC) were lower in rivers from lava fields, and higher in nonvolcanic subcatchments. Stable carbon isotope signatures ($\delta^{13}C$) of POC and DOC mean $\delta^{13}C$ of $-22.5‰$ and $-23.5‰$, respectively, are the first data to be reported for the highland of the Congo River basin and showed a much higher C4 contribution than in lowland areas. Rivers of the VVP were net sources of CH_4 to the atmosphere (4–5052 nmol L^{-1}). Most rivers show N_2O concentrations close to equilibrium, but some rivers showed high N_2O concentrations related to denitrification in groundwaters. $\delta^{13}C$ signatures of dissolved inorganic carbon suggested magmatic CO_2 inputs to aquifers/soil, which could have contributed to increase basalt weathering rates. This magmatic CO_2-mediated basalt weathering strongly contributed to the high major cation concentrations and total alkalinity. Thus, chemical weathering (39.0–2779.9 t km^{-2} yr^{-1}) and atmospheric CO_2 consumption (0.4–37.0 $\times$ 10^6 mol km^{-2} yr^{-1}) rates were higher than previously reported in the literature for basaltic terrains.

1. Introduction

Rivers transport dissolved and particulate matter from land to the oceans. Part of the solutes transported by rivers are derived from chemical weathering processes in the catchment that is a function of local lithology, climate, and topography [*Ludwig et al.*, 1996; *Gaillardet et al.*, 1999; *Hartmann et al.*, 2014]. Part of the particulate load is derived from mechanical weathering. The terrestrial biosphere and in particular soils provide particulate (POC) and dissolved (DOC) organic carbon to rivers. Groundwaters carry the products of aerobic and anaerobic mineralization in soils toward the river network, and along with mineralization of POC and DOC within the river system, this typically leads to large emissions of greenhouse gases (GHGs) such as carbon dioxide (CO_2) [*Raymond et al.*, 2013; *Lauerwald et al.*, 2015; *Borges et al.*, 2015] and methane (CH_4) [*Bastviken et al.*, 2011; *Borges et al.*, 2015]. Anthropogenic inputs of nitrogen from fertilizers or wastewater can lead to high N_2O emissions from rivers to the atmosphere that are commonly attributed to denitrification [*Beaulieu et al.*, 2010a; *Baulch et al.*, 2011; *Marwick et al.*, 2014]. Nitrogen-poor rivers on the other hand have low N_2O levels [*Baulch et al.*, 2011; *Borges et al.*, 2015].

The annual global CH_4 emissions to the atmosphere between 2000 and 2009 have been estimated at ~548 Tg CH_4 yr^{-1}; of which 218 Tg CH_4 yr^{-1} were from natural sources and 335 Tg CH_4 yr^{-1} from anthropogenic sources [*Kirschke et al.*, 2013]. Of the fluxes from natural sources, 175 Tg CH_4 yr^{-1} were from natural wetlands and 43 Tg CH_4 yr^{-1} from other natural sources, i.e., freshwater, geological processes, oceans, wild animals, wildfire, and termites [*Pison et al.*, 2009; *Bousquet et al.*, 2011; *Beck et al.*, 2012; *Fraser et al.*, 2013]. Approximately 49% of the global CH_4 emissions from freshwater ecosystems is thought to occur in the tropics [*Bastviken et al.*, 2011].

Raymond et al. [2013] provided global CO_2 evasion rates of 1.8 Pg C yr^{-1} from streams and rivers, and 0.3 Pg C yr^{-1} from lakes and reservoirs which is highly significant when compared to the land biosphere and oceanic carbon sink of 2.0 Pg C yr^{-1}, respectively [*Le Quéré et al*., 2014]. The emission from rivers and streams has been recently revised downward to $<$0.7 PgC yr^{-1} by *Lauerwald et al*. [2015]. Yet in both these studies, the CO_2 data distribution in rivers and streams is skewed toward temperate and boreal systems in the Northern Hemisphere, while little data are available at tropical latitudes. There has been a growing number of studies of GHG fluxes in African rivers [*Koné et al*., 2010; *Bouillon et al*., 2009; 2012, 2014; *Mann et al*., 2014; *Marwick et al*., 2014; *Teodoru et al*., 2015], that combined with new data have contributed to evaluate for the first time the emissions of GHGs from inland water at the African continental scale [*Borges et al*., 2015]. The CO_2 and CH_4 emissions from African inland waters were found to be significant at both regional and global scales, totaling 0.4 Pg C yr^{-1} for river channels alone, and 0.9 Pg C yr^{-1} for river channels and wetlands of the Congo [*Borges et al*., 2015].

Volcanic fields are characterized by dry gas emissions which dissolve in the near-surface groundwaters and could thus contribute to the regional aquatic C pool. Despite this distinctive feature, streams and rivers of volcanic zones are still under-investigated for GHG evasion estimates. Volcanic terrains also act as an atmospheric C sink through chemical weathering. Thus, chemical and physical weathering is an important part of many elements cycles. On a global scale, atmospheric CO_2 consumption by chemical weathering leads to the storage of 237–288 Mt C yr^{-1} in surface waters and the oceans [*Amiotte-Suchet and Probst*, 1995; *Amiotte-Suchet et al*., 2003; *Gaillardet et al*., 1999; *Munhoven*, 2002; *Hartmann et al*., 2009; *Moon et al*., 2014]. About 63% of this global estimate is due to silicate weathering [*Hartmann et al*., 2009]. Basalt weathering represents 30–35% of CO_2 sequestred by silicate weathering [*Gaillardet et al*., 1999; *Dessert et al*., 2003], although basalts correspond to only 4–6% of the global continent area [*Meybeck*, 1987; *Amiotte-Suchet et al*., 2003; *Hartmann et al*., 2009]. Given the large quantity of sequestrated C and the subsequently significant role on climate regulation, more studies are needed to improve the quantification of chemical weathering and CO_2 consumption in basaltic formations. Investigating weathering rates in basaltic terrains at the regional scale contributes to reduce uncertainties in the modeling of the global atmospheric CO_2 consumption rate.

This study focuses on the geochemistry of rivers of the Virunga Volcanic Province (VVP) (Figure 1), characterized by high volcanic activity, located in a tropical climate zone, and with a dense hydrographic network, but which remains poorly studied from a geochemical point of view. We concentrated on the geochemical characterization of the major rivers of the VVP by: (1) quantifying concentrations of nutrients, major cations, organic and inorganic carbon and their stable carbon isotope composition ($\delta^{13}C$); (2) the quantification of riverine CH_4 and N_2O concentrations and (3) the estimation of spatial variations of these parameters. We additionally quantified solutes and suspended material fluxes, the chemical weathering rates and the associated atmospheric CO_2 consumption during basalt weathering. Finally, the dependence at regional scale of chemical weathering on climatic factors (temperature and runoff) was discussed.

2. Study Area

2.1. Geological and Hydrological Settings

The VVP is located in the western branch of the East African Rift and is bounded on the north by Lake Edward, on the south by Lake Kivu, the Rwandan dorsal on the east and the Mitumba Range on the west (Figure 1). Virunga volcanic activity started during the mid-Miocene [*Pouclet*, 1977] and consists of eight major volcanic edifices perpendicularly aligned to the position of the rift. Most edifices are dormant except Mount Nyiragongo (4370 m) and Mount Nyamulagira (3058 m), both located in the Democratic Republic of the Congo (DRC) and are the Africa's most active volcanoes. The edges of the rift are difficult to detect due to intense erosion, important vegetation cover and frequent lava flows [*Smets*, 2007] especially in the east. Nearly all the Virunga lavas are of alkalic to highly alkalic composition (Table 1), the alkalic character varies from a relatively sodic pole [$Na_2O > K_2O$] to a potassic or hyperpotassic pole [$K_2O \gg Na_2O$]. The VVP consists of plains, shelf, and mountain ranges with altitudes of 900 m in the basin of Lake Edward and 1460 m in the Lake Kivu basin. The highest point is the Mount Karisimbi summit at 4508 m (Figure 1). The alluvial plain extends over the south basin of Lake Edward (i.e., lacustrine of Figure 2b), and then steadily rises up toward the Nyamulagira and Nyiragongo lava flows (i.e., basalt/volcanic ash of Figure 2b). The boundary

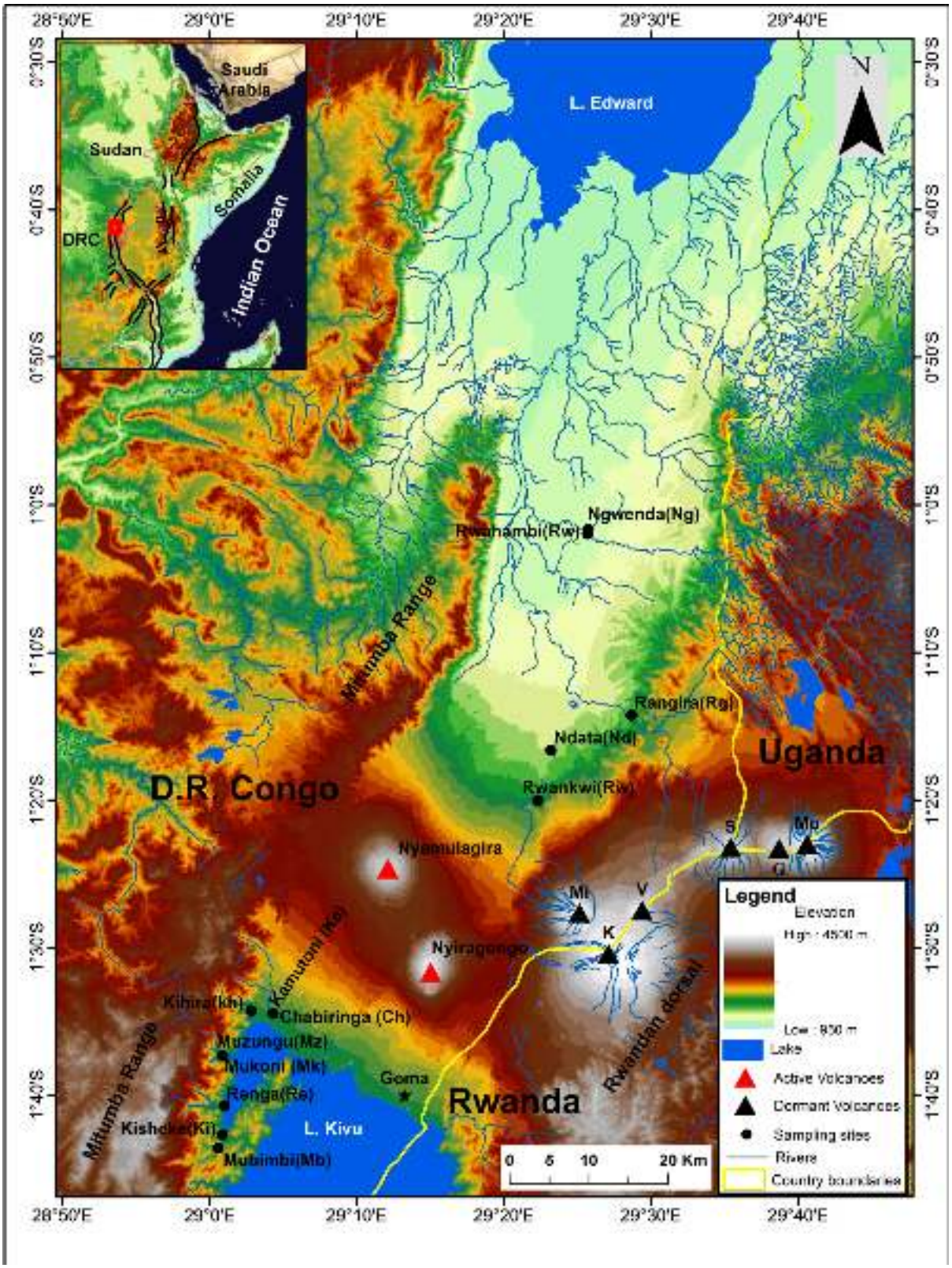

Figure 1. Map of the Virunga Volcanic Province (VVP) showing the sampling sites. Eight of the 13 sampled rivers drain into the Kabuno bay (a subbasin of Lake Kivu), i.e., Mubimbi (Mb), Kisheke (Ki), Renga (Re), Mukoni (Mk), Muzungu (Mz), Kihira (Kh), Kamutoni (Ka), and Chabiringa (Cha). The five others rivers drain into Lake Edward catchment, i.e., Rwankwi (Rk), Ndata (Nd), Rangira (Ra), Rwahambi (Rw), and Ngwenda (Ng). The blue lines represent the hydrographic network by *BEGo (Synoptics, Keyobs, Royal Museum for Central Africa, Catholic University of Louvain)* [2005]. The map also shows the six dormant volcanoes of the Virunga, i.e., Mikeno (Mi), Karisimbi (K), Visoke (V), Sabinyo (S), Gahinga (G), and Muhabura (Mu) while Nyiragongo and Nyamulagira are still active. The black lines in the inset map display the boundaries of the East African Rift System.

Table 1. Major Elements Composition (wt %) of the Virunga Lavas

	Nyiragongo[a] Mean (Range)	Nyamulagira[b] Mean (Range)	Mikeno[c]
SiO_2	38.92 (29.72–48.38)	45.59 (37.88–47.83)	47.23
Al_2O_3	14.22 (10.60–19.90)	14.08 (8.42–18.68)	15.01
Fe_2O_3	11.73 (4.88–17.50)	5.07 (0.24–10.8)	9.91
FeO	6.46 (0.97–9.33)	8.64 (3.07–10.59)	
MnO	1.30 (0.16–6.30)	0.19 (0.03–0.35)	0.18
MgO	3.89 (0.16–6.30)	7.82 (0.19–14.9)	3.49
CaO	12.88 (8.11–18.86)	11.26 (5.16–18.09)	9.25
Na_2O	5.26 (1.90–7.28)	2.62 (1.5–11.38)	4.05
K_2O	5.11 (2.04–7.34)	2.93 (1.05–5.85)	6.28
TiO_2	2.87 (1.98–4.30)	3.27 (1.25–5.14)	3.04
P_2O_3	1.55 (0.44–2.39)	0.42 (0.13-2.09)	0.77
CO_2	1.69 (0.40–3.16)	0.11 (0–0.33)	
H_2O^+	0.52 (0.35–0.68)	0.33 (0–0.84)	0.69
H_2O^-	0.18 (0.12–0.24)	0.10 (0–0.64)	
$K_2O + Na_2O$	10.38	5.55	10.33
K_2O/Na_2O	0.97	1.11	1.55
Mg#	29.89 (22.80–32.74)	39.08 (34.53–43.3)	28.13

[a]Undated lavas, lava from the 1977 and 2002 eruptions, after *Demant et al*. [1994], *Platz et al*. [2004], *Chakrabarti et al*. [2009], and *Andersen et al*. [2012, 2014].

[b]Undated lavas, lava from the 1912, 1938, 1948, 1977, 1982, 1986, 2006, and 2010 eruptions after *Denaeyer* [1972, 1975], *Pouclet* [1974], *Aoki and Kurasawa* [1984], *Aoki et al*. [1985], *Hertogen et al*. [1985], *Marcelot et al*., 1989, *Head et al*. [2011], and *Smets et al*. [2013].

[c]*Guibert* [1978].

between the Lake Edward and Lake Kivu watersheds is located on the line connecting the Nyamulagira-Nyiragongo-Karisimbi volcanoes (W to E oriented line; Figure 1). This boundary also corresponds to the limit between the Congo River basin to the south and the Nile River in the North. The mountain climate that marks the region is controlled by the nearby equatorial forest of the Virunga National Park and the mountain range. Precipitation is estimated at 1400–1500 mm yr^{-1} [*Muvundja et al*., 2009], and the mean annual temperature at ~19.2°C. The region experiences a long wet season (September–May) and a dry season (June–August), with a short occasional dry season from mid-January to February. Lake Kivu (1460 m) and the hundreds of tributaries dominate the hydrography in the south of Virunga. The center and the north consist of a river network that feeds the Rutshuru River which flows into Lake Edward.

2.2. Soil Type and Land Uses

Three classes of soil are distinguished in the VVP (Figure 2a). The first lies on the area of presently active volcanoes and is composed of umbric and mollic andosols; the second covers the area of extinct volcanoes and composed of mollic andosols. The third consist of soil of alluvial and metamorphic rocks parent materials, formed by luvic phaeozems, haplic acrosols, and mumic cambisols (Figure 2a). The soils of presently active volcanic areas contain a thin humus layer covering lava flows on which mosses and lichens grow. A thick and slightly compact and humus-rich soil has developed on old lava flows; while the soil of the alluvial plain derives from sedimentary deposits. Local people practice traditional agriculture and livestock but an important area of the Virunga area is part of the Virunga National Park. No chemical fertilizers are used in the region. The lack of agricultural management on lands with steep slopes and the significant deforestation have generated substantial soil movements. They mainly include soil erosion and landslides, particularly in the mountainous watershed of Lake Kivu. The region is experiencing significant urbanization due to rural exodus triggered by repeated wars, causing Goma and the other small cities to host 4.2% of the population of the North Kivu province [*Document stratégique de réduction de la pauvreté* (*DSRP*), 2005].

3. Materials and Methods

3.1. Sampling Techniques

We carried out monthly sampling on 13 rivers in the VVP (all located in the DRC) from December 2010 to February 2013; eight are located in the Kabuno bay basin (a subbasin of Lake Kivu) while the five others drain into Lake Edward (Figure 1). Temperature, specific conductivity, pH, and dissolved oxygen (%O_2) were measured in situ with a Hanna (Hi 9828) multiparameter probe between December 2010 and December 2011,

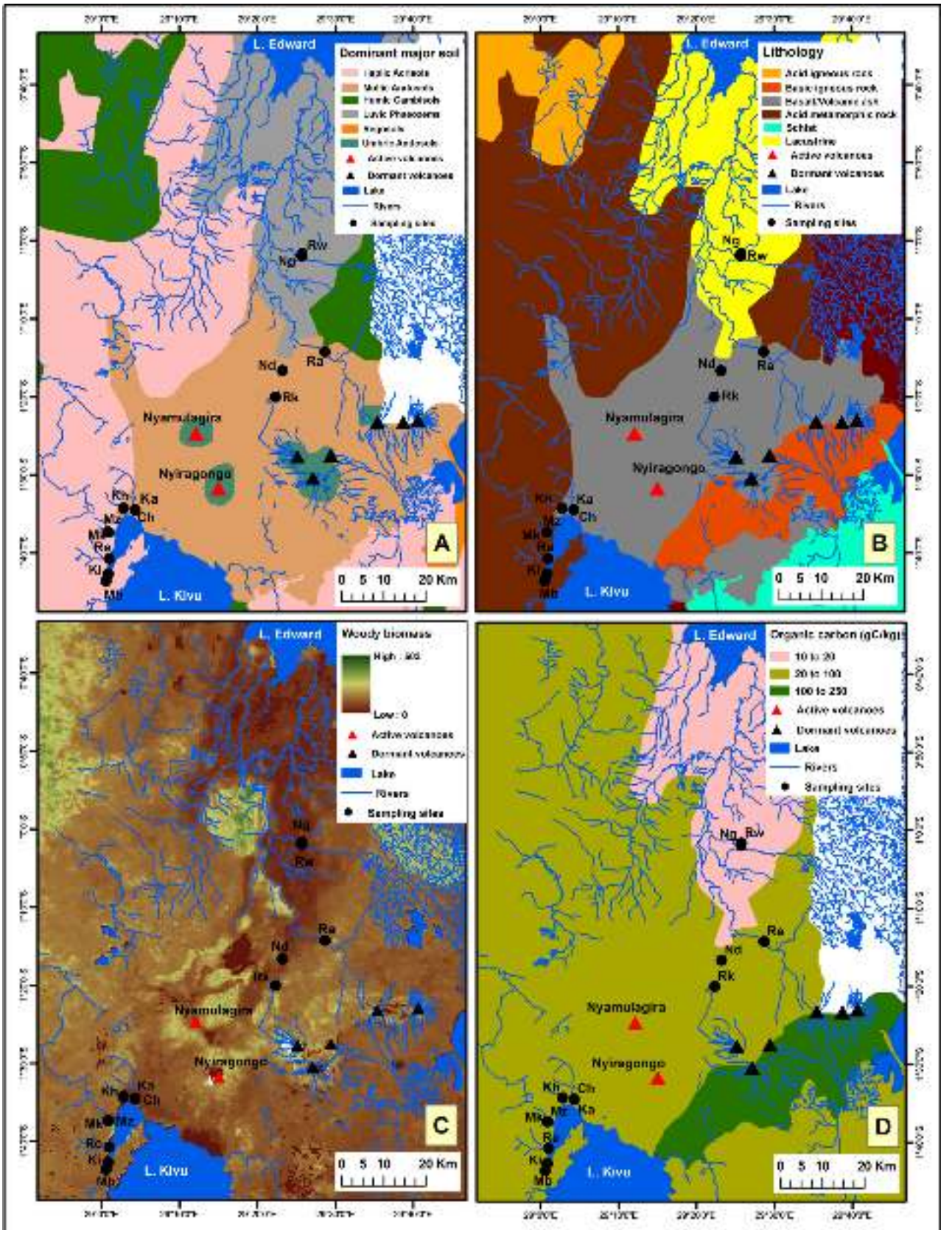

Figure 2. (a) Map of the major dominant soil groups, (b) lithology, (c) biomass, and (d) organic carbon distribution in the Virunga Volcanic Province.

and with an YSI ProPlus probe for the rest of the measurement period. The same calibration procedures were applied for both probes ensuring data continuity. Calibration of the pH electrode was carried out the evening prior to field measurements using pH 7.00 and pH 10.00 (25°C) standard buffers. The oxygen probes were calibrated with humidity-saturated ambient air in the field. Precision of conductivity, water temperature, pH, and $\%O_2$ was estimated to 1 μS/cm, 0.1°C, 0.01 pH units, and 0.5%, respectively. Water for the analysis of dissolved gases (CH_4 and N_2O) was collected in two glass serum bottles of 50 mL and poisoned with 200 μL of a saturated $HgCl_2$ solution, and sealed with butyl stoppers and aluminum caps. Samples for the measurement of the carbon isotopic composition in the dissolved inorganic carbon (δ^{13}C-DIC) were stored in 12 mL Exetainer vials and preserved with 100 μL of saturated $HgCl_2$ solution. Water for total alkalinity (TA), major elements, dissolved organic carbon (DOC), and its δ^{13}C signature was filtered through a 0.2 μm pore size polysulfone syringe filters, after prefiltration on 0.7 μm glass fiber filters. TA samples were collected in 50 mL high-density polyethylene bottles, 20 mL scintillation vials were used for major ions and preserved with 50 μL of HNO_3 65%, while samples for DOC and $\delta^{13}C_{DOC}$ were collected in 50 mL Supelco glass bottles with polytetrafluoroethylene-coated septa, and preserved with 50 μL concentrated H_3PO_4. Samples for total suspended matter (TSM), particulate organic carbon (POC) and its δ^{13}C signature, and for particulate nitrogen (PN) were obtained by filtering a known volume of water (between 700 and 1700 mL depending on the turbidity of the river) through Macherey-Nagel GF-5 47mm precombusted (5 h at 500°C) glass fiber filters. Two 50 mL plastic bottles were filled with water from the Macherey-Nagel GF-5 filtration, preserved with 200 μL of H_2SO_4 4 N for nitrates (NO_3^-), nitrites (NO_2^-), ammonium (NH_4^+), and soluble reactive phosphorus (SRP) determination. For total phosphorus (TP) determination, a 50 mL plastic bottle was filled with unfiltered water and preserved with 200 μL of 4 N H_2SO.

3.2. Analytical Techniques

Concentrations of CH_4 and N_2O were determined by gas chromatography (GC) with flame ionization detection (SRI 8610C), after creating a 20 mL headspace with N_2 in the 50 mL glass serum bottle. A Flame Ionization Detector (FID) coupled to a Hayesep D column was used for CH_4 measurements, while an Electron Capture Detector (ECD) coupled to a Hayesep N column was used for N_2O measurements. The two detectors were calibrated at the start and end of each series with certified gas mixtures of 1, 10, and 30 μatm of CH_4 and 0.2, 2, and 6 μatm of N_2O (Air Liquide Belgium). The overall precision of measurements was ±3.9% and ±3.2% for CH_4 and N_2O, respectively [*Borges et al*., 2015]. Concentrations of dissolved CH_4 and N_2O were calculated based on the partial pressure of the gas, its volume in the headspace and the water volume according to standard procedures by *Weiss* [1981]. δ^{13}C-DIC was analyzed using an elemental analyzer-isotope ratio mass spectrometer (EA-IRMS, Thermo Flash EA/HT and DeltaV Advantage). First, a 2 mL Helium headspace was created in the sample which was then acidified with H_3PO_4 and equilibrated overnight. A subsample from the headspace was injected into the EA-IRMS, and data were corrected for isotopic fractionation between dissolved and gaseous CO_2 as described by *Gillikin and Bouillon* [2007]. Measurements were calibrated with LSVEC and either NBS-19 or IAEA-CO-1 reference materials. The reproducibility of δ^{13}C-DIC measurement was typically better than $\pm 0.2‰$. TA was determined by Gran titration method with 0.1 M HCl as titrant using an automated titrator (Metrohm 725 Dosimat) equipped with a pH probe (ORION 8102 SC). Data were quality checked with certified reference material obtained from Andrew Dickinson (Scripps Institution of Oceanography, University of California, San Diego, USA). Typical reproducibility of TA measurements was better than ±3 μmol L^{-1}. For DOC and $\delta^{13}C_{DOC}$ analysis, 9–15 mL of sample were analyzed using a wet oxidation DOC analyzer (Thermo Hiper TOC or Aurora 1030W) coupled to an IRMS (Delta +XL or Delta V Advantage), calibrated with IAEA-C6 and an internal sucrose standard ($\delta^{13}C = -26.99 \pm 0.04‰$) calibrated against international reference materials. Reproducibility of δ^{13}C-DOC was typically better than $\pm 0.2‰$ and relative standard deviation for DOC concentration measurement was always below ±5%. Major elements were measured with inductively coupled plasma mass spectrometry (ICP-MS; Agilent 7700x) calibrated with the following standards: SRM1640a from National Institute of Standards and Technology, TM-27.3 (lot 0412) and TMRain-04 (lot 0913) from Environment Canada, and SPS-SW2 Batch 130 from Spectrapure Standard. Limit of quantification was 0.5 μmol L^{-1} for Na^+, Mg^{2+}, and Ca^{2+}, 1.0 μmol L^{-1} for K^+ and 8 μmol L^{-1} for Si. TSM values were obtained as the ratio of sediment load to the filtered water volume, the sediment load being determined as the net weight of sediment collected on the precombusted GF-5 filters, after redrying, with a precision of ±0.2 mg L^{-1}. To measure the POC, δ^{13}C-POC and particulate nitrogen (PN), a cutout of 11 mm diameter was made in the GF-5 filter, carbonates were removed by exposure to concentrated HCl

fumes for at least 4 h, and these were redried and packed in Ag cups. Calibration of δ^{13}C-POC, δ^{15}N-PN, POC, and PN measurements was performed with acetanilide ($\delta^{13}C = -27.65 \pm 0.05‰$; $\delta^{15}N = 1.34 \pm 0.04‰$) and leucine ($\delta^{13}C = -13.47 \pm 0.07‰$; $\delta^{15}N = 0.92 \pm 0.06‰$) as standards. All standards were internally calibrated against the international standard IAEA-C6 and IAEA-N1. Reproducibility of δ^{13}C-POC and δ^{15}N-PN measurement was typically better than $\pm 0.2‰$ and relative standard deviation for POC and PN measurement was always below 5%. Nutrients (NO_2^-, NO_3^-, NH_4^+, SRP, and TP) analysis was performed using a GENESIS 20 single beam spectrophotometer, according to standard colorimetric protocols following *Rodier and Bazin* [2005] and *American Public Health Association* [1998]. The detection limits were 0.3, 0.03, and 0.15 μmol L^{-1} for NH_4^+, NO_2^-, and NO_3^-, respectively.

3.3. GIS Analysis and Discharge Estimation

SRTM DEM (Shuttle Radar Topography Mission-Digital Elevation Model) data sampled at 3 arc sec (~30 m) pixel size were used to generate the topographical map of the VVP (Figure 1). The SRTM DEM data were collected by the NASA, the USA National Geospatial-Intelligence Agency, and the German and Italian space agencies joint team. A full description of the SRTM DEM data can be found in *Farr et al*. [2007]. Maps of the dominant major soil groups (Figure 2a) and organic carbon distribution (Figure 2d) were produced using data from the FAO SOTWIScaf, ver. 1.0, a central Africa soil features described in *Batjes* [2008]. The spatial distribution of the aboveground live woody biomass (Figure 2c) was extracted from the Pantropical National Level Carbon Stock Dataset for tropical countries [*Baccini et al*., 2008]. Land cover (supporting information Figure S1) data were extracted from the FAO *GLCN2000* [*Global Land Cover 2000 database*, 2003] (Global Land Cover Network) database for Africa, which is at ~300 m resolution and described in *Mayaux et al*. [2004]. The hydrographic network (Lake and rivers) is taken from the Building Environment for the Gorilla's [*BEGo (Synoptics, Keyobs, Royal Museum for Central Africa, Catholic University of Louvain)*, 2005]. Lithology (Figure 2b) is based on the GLiM (Global lithological map) from *Hartmann and Moosdorf* [2012].

The drainage areas (supporting information Figure S2) were derived from a high-resolution DEM computed by the HydroSHEDS mapping product (http://hydrosheds.cr.usgs.gov/index.php) and using the ArcHydro 2.0 Toolbox for ArcGis 10.2 software. Monthly discharges (supporting information Data Set S1) were estimated using an approach based on DEM and local precipitation data. The DEM grid was used to successively extract flow direction and flow accumulation grids. The latter represents the number of upslope cells that flow into each cell, and thus can be used to derive stream networks. The flow accumulation grid was converted into an accumulated area grid by multiplying the flow accumulation grid by the DEM grid resolution (here 92.43 m^2). Then, multiplying the value of the accumulated area determined at the outlet of a basin by a value of precipitation results in a measure of accumulated runoff per unit of time. Average monthly precipitations (supporting information Data Set S1) for each basin are derived from the 1 km^2 resolution WordClim Database [*Hijmans et al*., 2005]. A comparison of the results obtained using this approach with the data from 10 USGS gauges across the U.S.A. provided satisfactory results [*Wieczorek*, 2012].

3.4. Annual Load and Weathering Rate Estimation

Discharge-weighted mean concentrations were calculated in order to avoid dilution and evaporation effects on the annual loads and weathering rates. For a given parameter, the discharge-weighted mean concentration (C_w) was calculated as follows:

$$C_w = \frac{\sum_{i=1}^{n} C_i \times Q_i}{\sum_{i=1}^{n} Q_i}$$

where C_i is the monthly measured concentration and Q_i the calculated monthly discharge.

The estimated monthly discharges can be found in the supporting information. The annual load was then obtained by multiplying the discharge-weighted mean concentration (C_w) with the annual discharge. Following the same procedure, atmospheric CO_2 consumption rate was estimated from the discharge-weighted mean HCO_3^- (TA) concentration, based on the assumption that HCO_3^- is generated by silicate rock weathering, as confirmed by analysis of major element property-property plots (see hereafter). The mechanical weathering rate was estimated from discharge-weighted mean TSM concentration. The cationic weathering rate was estimated from the sum of major cations ($TDS_{cat} = \sum$ Ca, Mg, Na, and K). The chemical weathering rate was estimated from the total dissolved solid (TDS_{cond}), the latter calculated from specific

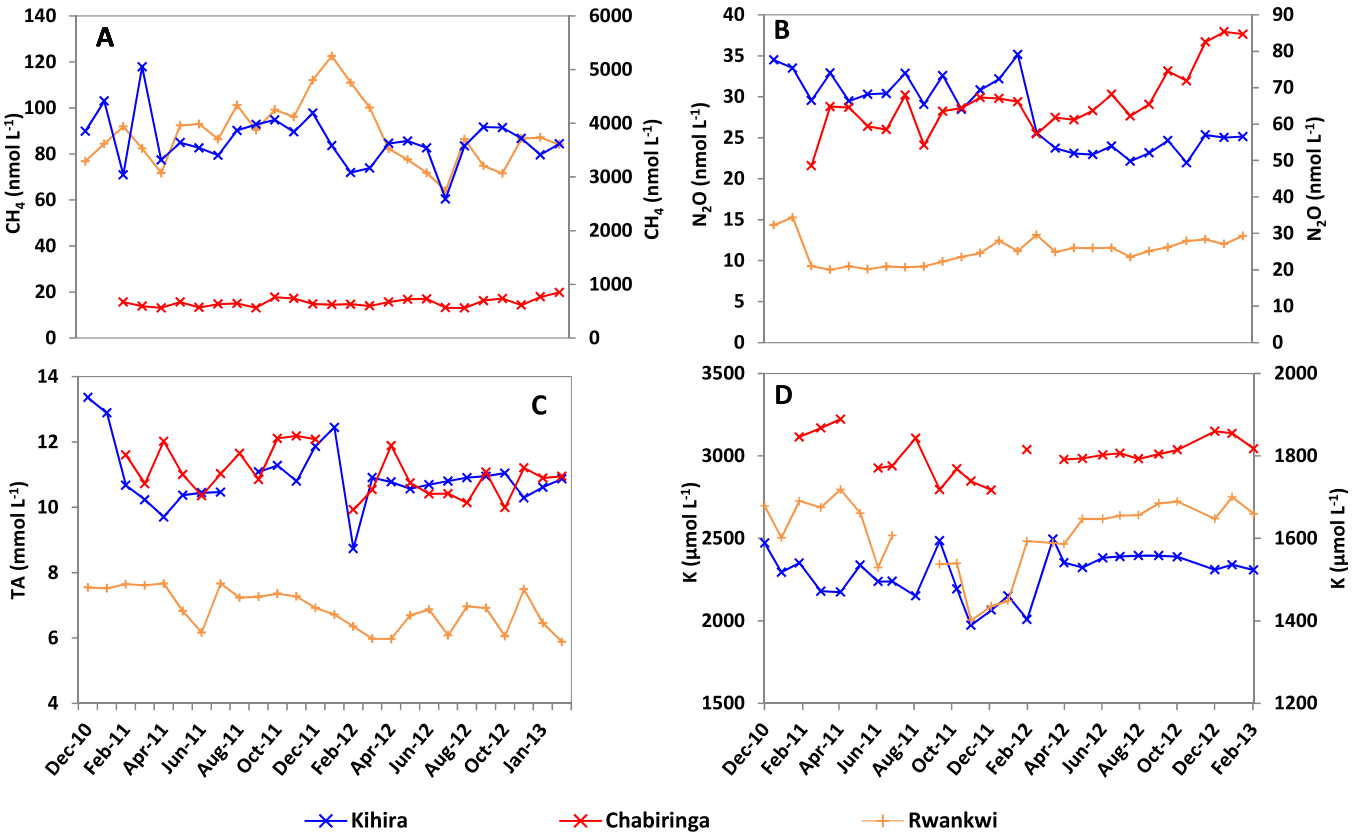

Figure 3. (a) Temporal variation of methane, (b) nitrous oxide, (c) total alkalinity, and (d) K^+ concentrations in a selection of the sampled rivers of the Virunga Volcanic Province between December 2010 and February 2013. Kihira in Figure 3a, Chabiringa in Figure 3b, and Rwankwi in Figure 3d are referred to the right axes.

conductivity as described in *Atekwana et al.* [2004]. All fluxes and weathering rates are expressed on an areal basis, i.e., by dividing the annual load with the river catchment area.

Major cations concentrations were corrected for atmospheric inputs using data from *Cuoco et al.* [2012a] which studied rainwater chemistry in the VVP between 2004 and 2010. Only data from rain samples collected to the N-NE and the W-SW of Mt Nyiragongo were considered. Samples from Nyiragongo crater and surrounding were not considered as they were not included in the drainage basins of this study. Furthermore, this area is impacted by the plume from Nyiragongo's permanent lava lake, and would thus only represent a source of error.

4. Results and Discussion

Most measured physicochemical and chemical features showed no well-defined seasonality (e.g., Figure 3 and supporting information Data Set S2). The mean temperature for each river throughout the study period ranged between 17 and 29.4°C (Figure 4a). Temperature was almost constant in Chabiringa and Kamutoni, while the other rivers showed a relative increase during dry season period, i.e., mid June to August. Shallow rivers showed important temperature fluctuations except for the Rwankwi which is supplied with high altitude water. No large DOC and POC increases were observed during the rising stage of runoff (mid-September to October) after the dry season, in contrast to what was observed in very large rivers such as the Oubangi River in the Congo River basin or other large tropical rivers [*Meybeck*, 2005; *Bouillon et al.*, 2012]. Thus, the POC/DOC, HCO_3^-/DOC, and POC/PN ratios showed only minor variations over time.

Given the general lack of marked seasonal variations, we principally focus on spatial variations of parameters. Mean concentrations of studied parameters are presented in Figures 4 and 6, the full database can be found in supporting information Data Set S2.

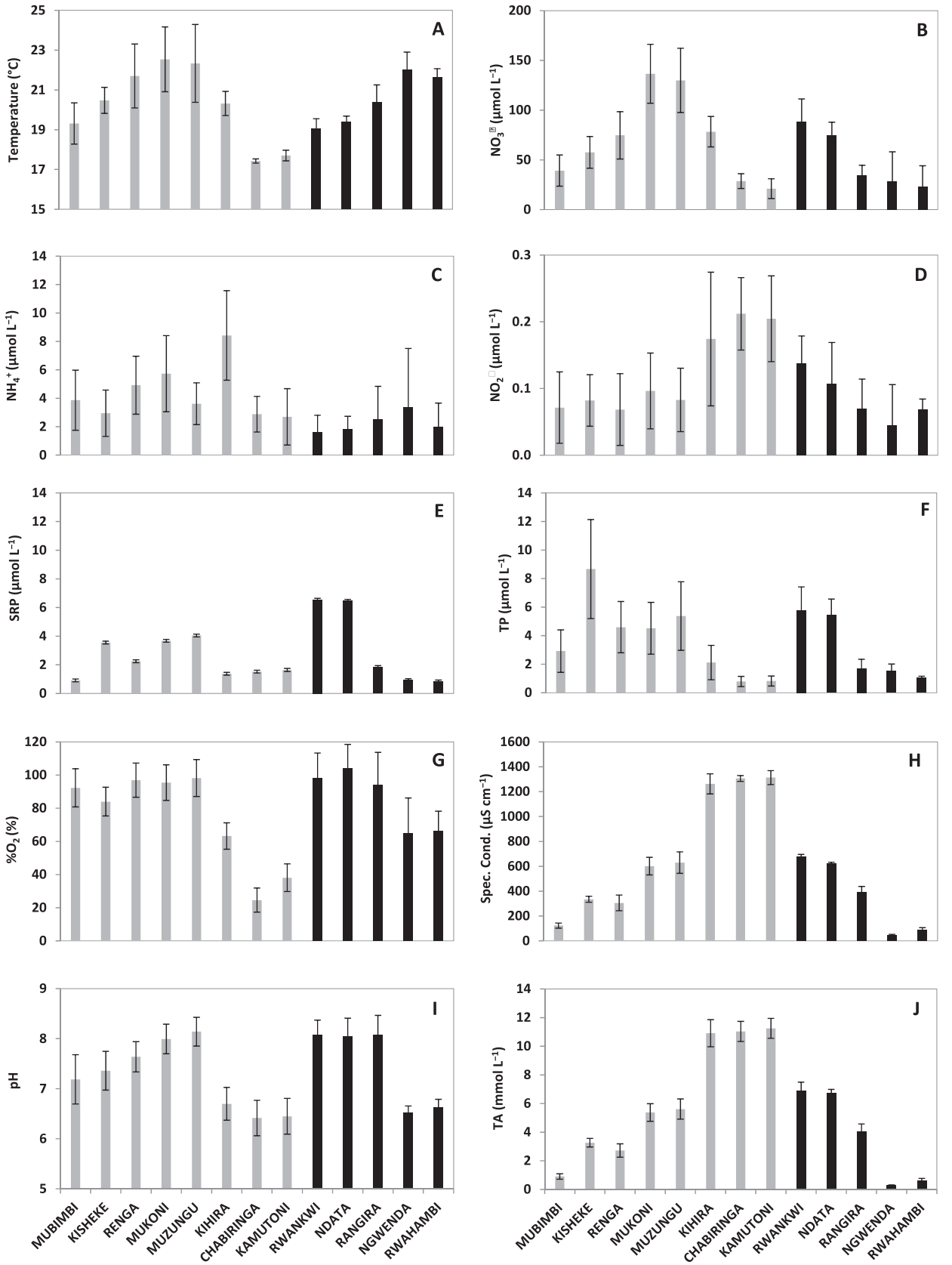

Figure 4. (a) Mean temperature, (b) nitrate, (c) ammonium, (d) nitrite, (e) soluble reactive phosphorus, (f) total phosphorus, (g) dissolved oxygen, (h) specific conductivity, (i) pH, and (j) total alkalinity in rivers of the Virunga Volcanic Province between December 2010 and February 2013. The gray and black bars represent rivers of Kabuno bay and Lake Edward catchment, respectively. The error bars represent one standard deviation.

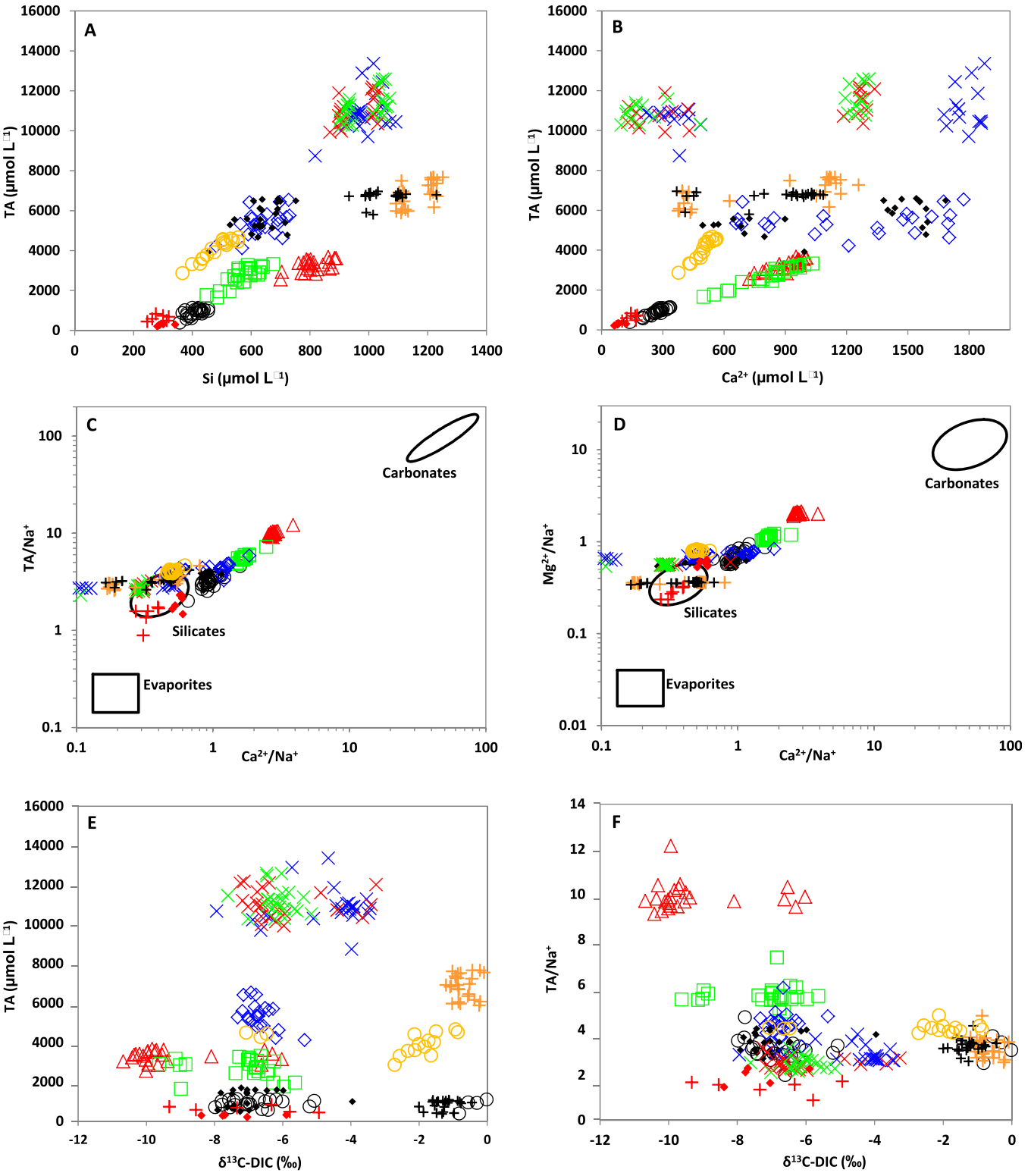

Figure 5. (a) Relationships between total alkalinity (TA) and Si, (b) TA and calcium, (c) TA/Na^+ and Ca^{2+}/Na^+, (d) Mg^{2+}/Na^+ and Ca^{2+}/Na^+, (e) TA and $\delta^{13}C_{DIC}$, and (f) TA/Na^+ and $\delta^{13}C_{DIC}$ in rivers of the Virunga Volcanic Province between December 2010 and February 2013. The Na^+ normalized plots show the composition fields for rivers draining different lithologies from a global compilation of the 60 largest rivers in the World [*Gaillardet et al.*, 1999].

4.1. Spatial Variations in Nutrient Concentrations

Monthly NO_3^- concentrations in the VVP rivers spanned a wide range (7–178 μmol L^{-1}), with large spatial variations (Figure 4b), and did not reach levels indicative of significant pollution or eutrophication. In parallel, the NH_4^+ and NO_2^- (Figures 4c and 4d, respectively) remained below the ranges normally found in unpolluted rivers (18 and 1.2 μmol L^{-1}, respectively) [*Meybeck*, 1982, 1983a]. The observed variations in the NO_3^-, NH_4^+, and NO_2^- concentrations were therefore of natural origin. On the other hand, mean SRP concentrations (Figure 4e) are higher compared to those of unpolluted rivers (10 μg L^{-1}) [*Meybeck*, 1982, 1993a], a discrepancy which could be related to a high degree of P mobilization during weathering of basaltic rocks (see below).

In rivers of the VVP, NH_4^+ represented between 1.5% and 11.9% of the total inorganic N pool, whereas NO_3^- largely dominated and accounted for 87.9–98.3%. This might suggest the conversion of NH_4^+ into NO_3^- through nitrification, leading to the dominance of NO_3^- over NH_4^+. The TP mean (Figure 4f) were slightly correlated to the SRP ($r^2 = 0.54$) and to NO_3^- ($r^2 = 0.33$). This implies the dominance of SRP in the P pool as SRP additionally represent >50% of TP in most rivers, and a possible common source for both P and N. In fact, P and N can be jointly mobilized from land runoff and groundwater.

Volcanic emissions are a possible source of nitrate and phosphate in active volcanic areas [*Julley et al*., 2008], and reach surface water through wet and dry deposits on the catchment. In the Virunga atmospheric inputs are important source of N and P, indeed *Muvundja et al*. [2009] found that total-N and total-P concentrations in atmospheric deposits were equal or larger than riverine values. P can also be produced in bioavailable form (P_4O_{10}) when hot lava reacts with water [*Vitousek*, 2004]. Like many other elements, P is released during chemical weathering. In the Japanese archipelago, P-release from silica-dominated lithology is estimated at a rate of 1–390 kg^{-1} km^{-2} yr^{-1} [*Hartmann and Moosdorf*, 2011]. Thus, even though P is a minor constituent of igneous rocks (mean from 0.42 to 1.55 wt % for the Virunga basalt; Table 1), volcanic products could be a minor source of P of VVP rivers.

Muvundja et al. [2009] reported nutrient data in Mukoni, Muzungu, Kihira, Chabiringa, and Kamutoni rivers during a monthly monitoring between October 2006 and July 2008. The SRP, Si, and TSM are comparable for both data sets. The higher NH_4^+ and TP values given by *Muvundja et al*. [2009] are possibly due to the difference in the sampling location, as they collected samples close to the mouth (near Kabuno bay) where contamination by wastewaters from villages along the course of the rivers may occur.

4.2. Major Cations and DIC Chemistry

Most rivers had mean O_2 concentrations near saturation, except Kamutoni and Chabiringa which were the most O_2-depleted waters, with means of 38.1% and 24.6%, respectively (Figure 4g), typical of high groundwater contributions as confirmed also by low temperature (Figure 4a) since they were sampled close to the resurgence points. The activity of the Nyamulagira seems to not influence temperatures of both rivers. The other rivers showed $\%O_2 > 60\%$ which implies important water oxygenation, given the steep slopes and shallow depths. Rwankwi, Ndata, and Mubimbi showed lower temperature (mean of ~19°C) associated with their high altitude origin on Mt Mikeno of the Virunga Nation Park (Rwankwi and Ndata) and the Mitumba Range (Mubimbi) (Figure 1). Specific conductivity data allow us to define three groups of rivers in the VVP: (1) the low mineralized (<150 μS cm^{-1}), (2) moderately mineralized (200–800 μS cm^{-1}), and (3) highly mineralized rivers with >800 μS cm^{-1} (Figure 4h).

The highly mineralized rivers, i.e., Kihira, Chabiringa, and Kamutoni are located on basaltic lithology in the field of active volcanoes, with a high major cation content and where the dominant cations are $Na^+ > K^+ > Mg^{2+} > Ca^{2+}$ (Table 2). This is a result of the intense weathering of basalt, mediated by magmatic CO_2 and the subsequent release of major cations to groundwater. The high alkalic composition of Virunga basalt promotes the dominance of Na^+ and K^+ in the cation composition of Kihira, Chabiringa and Kamutoni.

The moderately mineralized rivers are located in the field of dormant volcanoes to the NE and on nonvolcanic fields to the west (Figure 2b), where eruptive materials (i.e., ash, volcanic plume) were frequently deposited especially during Nyiragongo and Nyamulagira eruptions. Rwankwi and Ndata to the North-East, Mukoni and Muzungu to the West have similar specific conductivities (616–682 μS cm^{-1}) despite their location on different lithologies. The North-Eastern and Western rivers had different dominant cations

Table 2. Mean Cation Concentrations (Min-Max Between Parentheses) in Rivers of the Virunga Volcanic Province, Between December 2010 and February 2013

	Na (mM) Mean (Min-Max)	K (mM) Mean (Min-Max)	Mg (mM) Mean (Min-Max)	Ca (mM) Mean (Min-Max)	Si (mM) Mean (Min-Max)
Mubimbi	0.29 (0.15–0.39)	0.10 (0.07–0.16)	0.19 (0.12–0.23)	0.27 (0.14–0.34)	0.41 (0.36–0.45)
Kisheke	0.33 (0.23–0.37)	0.24 (0.12–0.30)	0.67 (0.47–0.74)	0.91 (0.72–1.00)	0.81 (0.70–0.89)
Renga	0.49 (0.29–0.69)	0.27 (0.20–0.33)	0.54 (0.34–0.71)	0.83 (0.50–1.03)	0.57 (0.45–0.68)
Mukoni	1.27 (0.83–1.66)	0.69 (0.53–1.00)	0.92 (0.69–1.05)	1.24 (0.66–1.77)	0.64 (0.48–0.73)
Muzungu	1.63 (1.03–1.92)	0.95 (0.72–1.13)	0.97 (0.54–1.14)	1.17 (0.50–1.69)	0.64 (0.45–0.75)
Kihira	3.72 (3.11–4.09)	2.28 (1.97–2.50)	2.49 (2.04–2.86)	1.12 (0.22–1.88)	0.99 (0.82–1.09)
Chabiringa	4.26 (1.62–4.71)	2.91 (0.88–3.22)	2.31 (0.97–2.55)	0.76 (0.13–1.43)	0.95 (0.69–1.03)
Kamutoni	4.49 (3.94–4.97)	3.08 (2.85–3.26)	2.44 (2.21–2.58)	0.73 (0.10–1.31)	0.99 (0.90–1.07)
Rwankwi	2.15 (0.26–0.55)	1.61 (0.04–0.11)	0.77 (0.08–0.14)	0.81 (0.10–0.17)	1.17 (0.25–0.32)
Ndata	2.05 (1.62–2.25)	1.41 (1.28–1.49)	0.73 (0.58–0.78)	0.84 (0.37–1.09)	1.05 (0.93–1.23)
Rangira	0.99 (0.74–1.15)	0.69 (0.53–0.81)	0.79 (0.60–0.93)	0.50 (0.38–0.56)	0.48 (0.37–0.56)
Ngwenda	0.15 (0.13–0.20)	0.05 (0.03–0.08)	0.09 (0.07–0.11)	0.08 (0.06–0.12)	0.30 (0.28–0.34)
Rwahambi	0.44 (1.57–2.34)	0.06 (1.40–1.72)	0.12 (0.56–0.83)	0.15 (0.38–1.26)	0.29 (1.09–1.25)

depending on the soil and the lithology of each watershed (Figures 2a and 2b). This highlights the secondary role of soil weathering to the river chemical composition in the VVP. Thus, Mukoni and Muzungu flowing on haplic acrisols (Figure 2a) were Na^+ and Ca^{2+} dominated; followed by K^+ and Mg^{2+} whose concentrations compete (Table 2). In contrast, Rwankwi and Ndata kept the K^+-Na^+ dominance related to the presence of extinct volcanoes in the catchments (Figure 2b). The low mineralized rivers are found on haplic acrisols to the West and luvic phaeozems to the North (Figure 2a) with the most diluted water at both extremities of the sampling zone, away from the influence of active volcanoes.

Mean pH varied from neutral to relatively acid or basic (6.4–8.1; Figure 4i). The mean TA ranged from low ($<$1.0 mmol L^{-1}) to exceptionally high ($>$10.0 mmol L^{-1}) values (Figure 4j). The TA was overall positively correlated to Si (Figure 5a), and showed a larger scatter as a function of Ca^{2+} (Figure 5b). This is indicative of a strong contribution of silicate rock weathering to TA (Figure 5a), and this is confirmed by the Na^+ normalized plots (Figures 5c and 5d). Both TA/Na^+ and Mg^{2+}/Na^+ versus Ca^{2+}/Na^+(Figures 5c and 5d, respectively) are aggregated to values close to those expected for silicate rock weathering based on the average values proposed by *Gaillardet et al*. [1999]. The rivers with a lithology dominated by acid metaphoric rocks (Mubimbi, Kisheke, Renga, Mukoni, and Muzungu) had a $Ca^{2+}/Na^{2+} > 1$, while the rivers with a lithology dominated by basalt/volcanic ash (i.e., Kihira, Chabiringa, Kamutoni, Rwankwi, Ndata, and Rangira; Figure 2b) were characterized by a $Ca^{2+}/Na^{2+} < 1$ and a TA/Na^+ close to 3. A few rivers (Kihira, Rwankwi, and Ndata) had Ca^{2+}/Na^+ values lower than the envelope of silicate rock end-member proposed by *Gaillardet et al*. [1999] (Figure 5c). This is probably related to the fact that *Gaillardet et al*. [1999] reported the chemical composition of the 60 largest rivers in the World, hence, excluding low mineralized small rivers such as some of those studied here. Another reason could be the atypical strong dominance of Na in the Virunga basalt, and consequently in the major cation composition of the stream network. The Na-normalized Ca^{2+} and Mg^{2+} ratios are consistent with high dissolution of Ca and Mg-rich silicate minerals, such as clinopyroxenes, mostly formed of diopside ($CaMgSi_2O_6$) [*Morimoto*, 1989] and which have been identified in Nyiragongo's basalt [*Platz*, 2002; *Platz et al*., 2004].

No consistent simple relationship was observed between TA and δ^{13}C-DIC (Figure 5e), but the river with the highest TA/Na^+ (Kisheke) was also characterized by the lowest δ^{13}C-DIC values (Figure 5f). Silicate weathering leads to the formation of HCO_3^- that has the isotopic signature of the CO_2 driving the weathering reaction. Since in freshwaters, DIC is usually dominated by HCO_3^-, especially in high TA systems, the δ^{13}C-DIC is close to the one of HCO_3^-, hence of the CO_2 initially involved in the dissolution of silicate rocks. Considering the evidence discussed above that silicate weathering is a strong contributor to TA in the region, the observed range of δ^{13}C-DIC (between $-10.7‰$ and $0‰$; Figure 6a) indicates that the CO_2 driving silicate weathering was not derived from organic matter mineralized in soils. Indeed, DOC and POC have a δ^{13}C signature ranging between $-28‰$ and $-18‰$ (Figures 6b and 6c, respectively). However, the range of river δ^{13}C-DIC matches well with the range of δ^{13}C of CO_2 in volcanic gases reported by *Deines* [2002]. We thus conclude that the δ^{13}C-DIC signatures are to a large extent influenced by volcanic CO_2 dissolution in groundwaters and involved in silicate rock weathering. This pattern is quite different from those observed

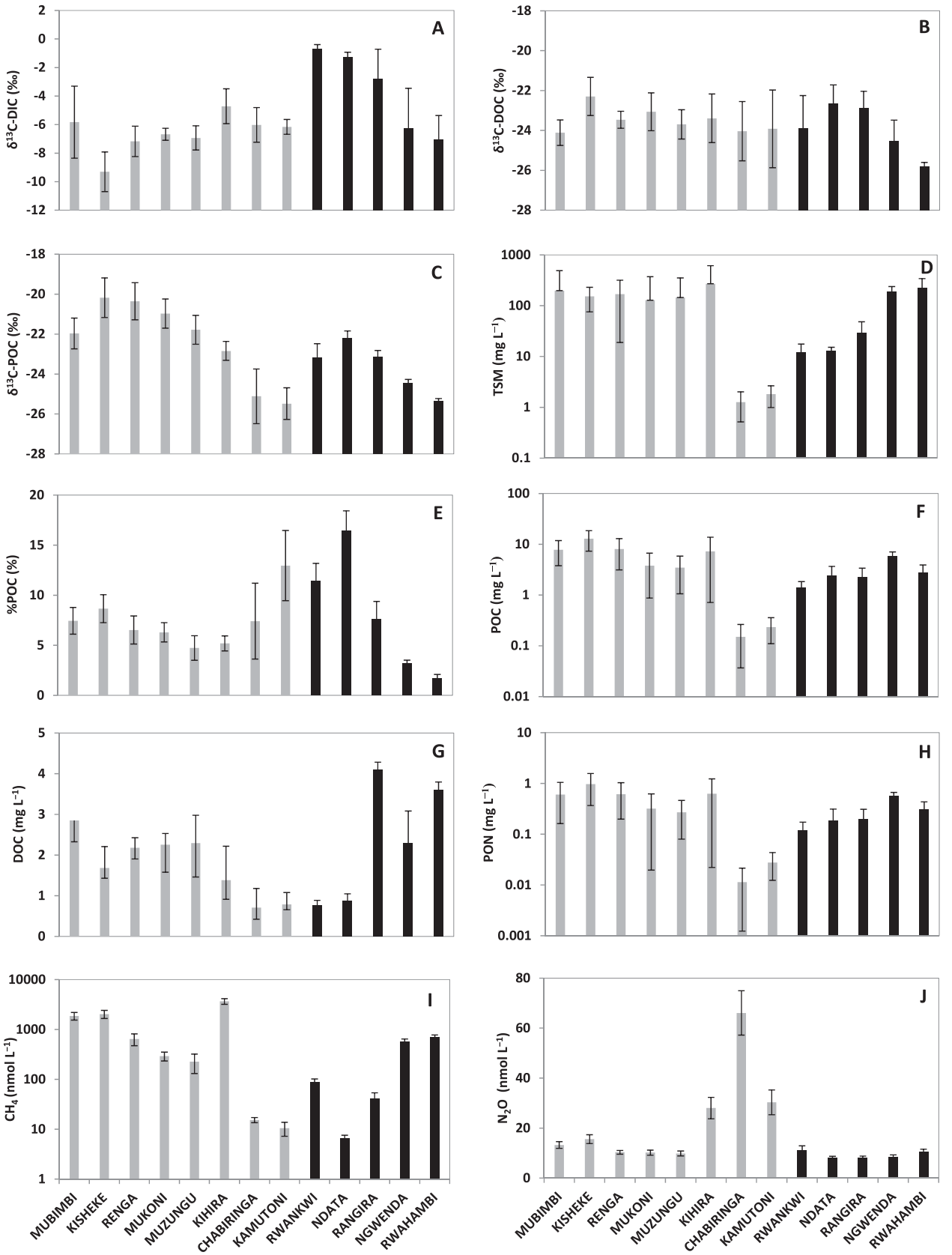

Figure 6. (a) Mean values of $\delta^{13}C_{DIC}$, (b) $\delta^{13}C_{DOC}$, (c) $\delta^{13}C_{POC}$, (d) total suspended matter, (e) %POC, (f) particulate organic carbon, (g) dissolved organic carbon, (h) particulate organic nitrogen, (i) methane, and (j) nitrous oxide in rivers of the Virunga Volcanic Province between December 2010 and February 2013. The gray and black bars represent rivers of Kabuno bay catchment and those of Lake Edward catchment, respectively. The error bars represent one standard deviation.

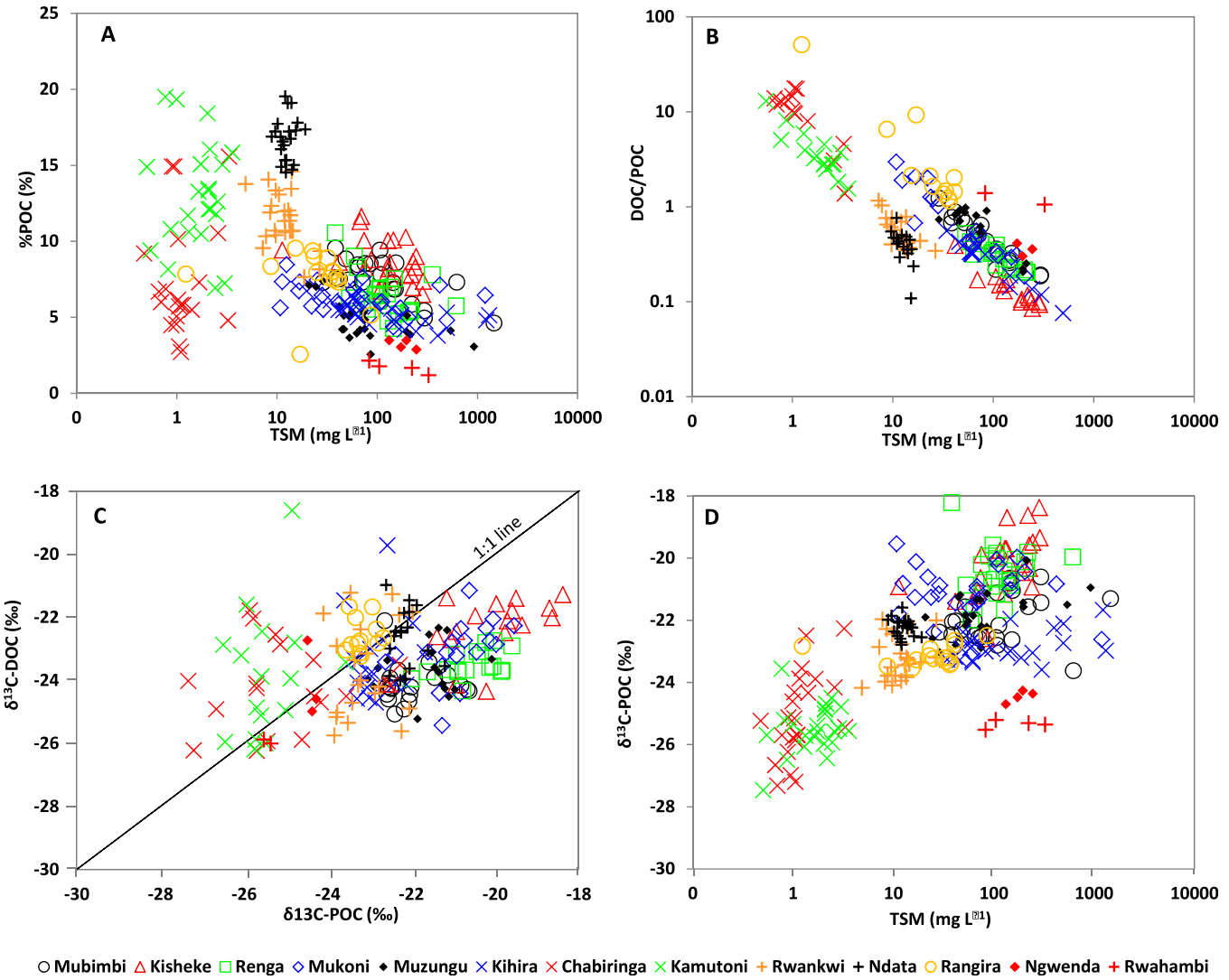

Figure 7. (a) Relationships between the %POC and total suspended matter, (b) DOC/POC and total suspended matter, (c) $\delta^{13}C_{DOC}$ and $\delta^{13}C_{POC}$, and (d) $\delta^{13}C_{POC}$ and TSM in rivers of the Virunga Volcanic Province between December 2010 and February 2013.

in the lower Congo basin, where δ^{13}C-DIC values as low as $\sim -26‰$ are found in rivers where silicate weathering also dominates, but where the CO_2 driving silicate weathering is produced by mineralization of organic matter derived from C3 vegetation [*Bouillon et al.*, 2014].

Silicate weathering also strongly affected the SRP distribution as shown by the highly significant correlation between SRP and dissolved Si (when the three headwater rivers Kihira, Chabiringa and Kamutoni are excluded) (Figure 8a). This is in line with the general link between P release and rock weathering [*Hartmann et al.*, 2014].

4.3. Organic Matter Dynamics and Origin

Large differences in the TSM load were observed in the VVP rivers. Higher TSM (289–1467 mg L^{-1}) was found in rivers located in the west of Kabuno bay basin, i.e., in Mubimbi, Kisheke, Renga, Mukoni, Muzungu, and Kihira (Figure 6d). These are second-order rivers draining a basin where steep slopes (supporting information Data Set S2), combined with high rainfall and agricultural land use practices, result in high erosion rates. The TSM load of these rivers is characterized by a relatively low organic matter content (mean %POC $<$ 9%, Figure 6e). The catchment of Kabuno bay is composed of haplic acrisols (Figure 2a) which are clay-enriched soils. The land is mainly used for farming (crops and pastures; supporting information Figure S1) which

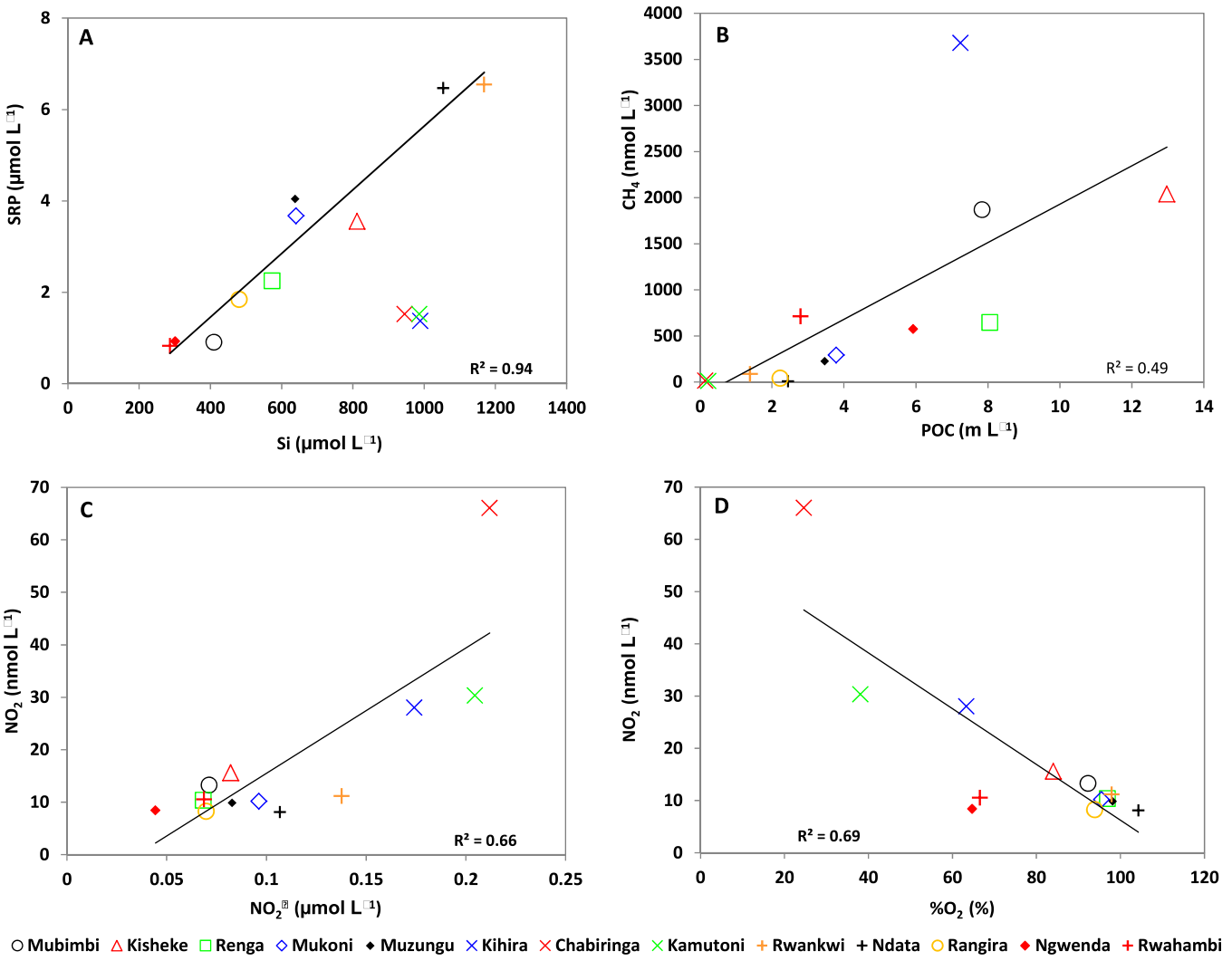

Figure 8. (a) Relationships between mean soluble reactive phosphorus and silicon, (b) mean methane and particulate organic carbon, (c) mean nitrous oxide and nitrite, and (d) between mean nitrous oxide and dissolved oxygen in rivers of the Virunga Volcanic Province between December 2010 and February 2013.

promotes soil erosion. Chabiringa, Kamutoni, Rwankwi, Ndata, and Rangira showed the lowest TSM, with values ranging from 0.5 to 86.3 mg L^{-1} (Figure 6d). These rivers flow on mollic andosols of volcanic parent material from the Nyamulagira and Mikeno volcanoes (Figure 2a), with shrubs or forest cover (supporting information Figure S1). Thus, the lower TSM observed in the rivers draining volcanic fields are a result of the lower sensitivity of volcanic rocks toward mechanical erosion processes. The TSM could however be potentially enriched in organic matter (%POC > 10, e.g., in Kamutoni, Rwankwi, and Ndata; Figure 7a) from the dense vegetation cover. Ngwenda and Rwahambi flow on luvic phaeozems which are humic-rich and highly productive soils. The latter have favored the development of farming activities that generate high TSM with a low %POC (Figure 7a) found in Ngwenda and Rwahambi.

Most Virunga rivers have mean TSM and POC (Figure 6f) that are higher than main stem Congo River (26.3 mg/L for TSM, 1.7 mg/L for POC) [*Coynel et al.*, 2005] or other large rivers [*Meybeck*, 1982; *Spitzy and Leenheer*, 1991; *Martins and Probst*, 1991]. Mean TSM loads in the VVP rivers draining mountainous catchments (128.3–270.4 mg L^{-1}) were also higher compared to volcanic mountainous rivers of Guadeloupe (11.8–56.2 mg L^{-1}) [*Lloret et al.*, 2013]. Nevertheless, Guadeloupe rivers have mean TSM somewhat high than that of Virunga rivers draining basaltic field (1.3–29.8 mg L^{-1}). POC concentrations were extremely variable among rivers, while DOC showed lower spatial variability (Figure 6g). In the majority of rivers, POC dominated the organic C pool. Differences in the POC/DOC ratios can be explained by differences in soil type, soil leaching and/or erosion and the relief. Both lower mean DOC (<0.9 mg L^{-1}) and POC

($<$2.5 mg L^{-1}) were observed in rivers draining volcanic fields (Figure 2a). These rivers (i.e., Chabiringa, Kamutoni, Rwankwi, and Ndata rivers) are characterized by low terrestrial biomass (Figure 2c) and low organic C soil content (Figure 2d).

The total organic C (TOC = DOC + POC) generally increased as one moves away from the volcanic area toward the NE and W. Thus, the TOC was found to be 6 to ~20 times higher in the most remote rivers. While DOC has typically been suggested to be the dominant C pool in large tropical rivers [*Meybeck*, 1993b], C of rivers of the VVP was largely DIC dominated. This is due to the high rates of silicate weathering and magmatic CO_2 inputs. The DOC/DIC ratios were below those of rivers draining carbonate rocks ($<$0.2) [*Meybeck*, 2005].

There was no straightforward relationship between the riverine POC and DOC and the vegetation or soil organic carbon distribution in the catchments. For instance, Rwahambi had among the highest mean DOC, and yet was draining catchment of both low organic C soil (Figure 2d) and woody biomass (Figure 2c). In contrast, DOC/POC ratios were well correlated to TSM (Figure 7b), with ratios above 1 (dominance of the DOC in the TOC pool) in the headwater streams (e.g., Chabiringa and Kamutoni). POC became dominant in more erosive and turbid systems as previously described in other studies [e.g., *Meybeck*, 1982; *Ittekkot and Laane*, 1991; *Ralison et al*., 2008; *Bouillon et al*., 2009]. Mean DOC, POC, and PN (Figure 6h) in the VVP rivers were almost similar to those reported by *Lloret et al*. [2013] for Guadeloupan rivers of volcanic fields (0.69–2.25, 0.98–6.70, 0.1–2.31 mg L^{-1}, respectively, for DOC, POC, and PN). Natural vegetation in the Virunga consists of a mixture of Hatch-Slack photosynthetic pathway plants (C4) and grasslands employing Calvin pathway (C3), with the former dominating in quantity [*Still and Powell*, 2010] (supporting information Figure S1). Agricultural practices have introduced both new C4 (e.g., maize, sorghum, sugar cane, etc.) and C3 (e.g., banana, potato, cassava, etc.) plants. Thus, Virunga riverine δ^{13}C-DOC (Figure 6b) and δ^{13}C-POC (Figure 6c) showed a mixed origin for organic C, from both C3 and C4: C3 plants have a typical δ^{13}C around $-30‰$ to $-26‰$, while C4 plants show a δ^{13}C of $\sim-12‰$ ($-10‰$ to $-14‰$) [*Ehleringer*, 1991]. We found however a slight dominance of C3-derived C to the riverine organic C pool, with mean δ^{13}C-DOC and δ^{13}C-POC of $-23.5‰$ and $-22.5‰$, respectively. There were no clear relationships between individual paired δ^{13}C-DOC and δ^{13}C-POC data, indicating both C pools were not closely coupled (Figure 7c). Literature data on the δ^{13}C of riverine POC and DOC in the Congo Basin are only available for low-altitude regions [e.g., *Mariotti et al*., 1991, *Spencer et al*., 2012, *Bouillon et al*., 2012, 2014], and show much more limited C4 contributions than those found in Virunga highlands, with the majority of data ranging between $-30‰$ and $-26‰$.

As also reported in the lowland Congo [*Bouillon et al*., 2014], the δ^{13}C-POC was positively correlated to TSM (Figure 7d) and might indicate higher sediment inputs in catchments where C4 vegetation (grassland) is more substantial. The negative relationship between %POC and TSM (Figure 7a) has been previously observed within a given catchment [*Tamooh et al*., 2012; *Bouillon et al*., 2014] or globally across catchments [*Meybeck*, 1982]. This pattern is typically driven by the combination of inputs from direct litter or organic-rich surface soil layers (high %POC-low TSM) and more soil-derived sediments (low %POC-high TSM).

4.4. CH_4 and N_2O

Virunga rivers were sources of methane to the atmosphere as most rivers of the world [*Bastviken et al*., 2011], the observed CH_4 concentrations (Figure 6i) were above atmospheric equilibrium (~2 nmol L^{-1}). Overall there was a positive relationship between CH_4 and POC (Figure 8b) driven by enhanced in situ CH_4 production fuelled by the availability of organic matter and the removal of both POC and CH_4 in groundwaters.

In contrast, only Chabiringa, Kamutoni, and Kihira were sources of N_2O to the atmosphere as they showed concentrations (Figure 6j) above the atmospheric equilibrium (~10 nmol L^{-1}). Two of these rivers (Chabiringa and Kamutoni) showed low CH_4; while the third (Kihira) had the highest CH_4 of all rivers sampled. Chabiringa and Kamutoni were sampled close to springs, and therefore have chemical characteristics close to those of groundwaters such as high TA, conductivity and major cation concentrations, and low pH, temperature, DOC, and POC concentrations. These rivers were also characterized by low NO_2^- and high N_2O which might be indicative of denitrification in the groundwaters. These features drive the positive correlation between N_2O and NO_2^- (Figure 8c) and the negative correlation between N_2O and $\%O_2$ (Figure 8d). Chabiringa and Kamutoni were also characterized by lower CH_4 concentrations indicative of CH_4 removal by bacterial oxidation in the groundwaters [*Borges et al*., 2015].

Table 3. Estimated Annual TSM, POC, PON, DOC, Si, and Nutrient Fluxes in Rivers of the Virunga Volcanic Province

	TSM (10^3 t/yr)	POC (t/yr)	PON (t/yr)	DOC (t/yr)	Si (t/yr)	NO_3^- (t/yr)	NO_2^- (t/yr)	NH_4^+ (t/yr)	SRP (t/yr)	Total P (t/yr)
Mubimbi	20.79	793.33	60.38	290.56	1061.75	231.31	0.34	6.63	2.55	8.67
Kisheke	1.47	121.56	9.03	15.23	196.87	29.43	0.03	0.48	0.84	2.37
Renga	13.10	661.38	46.96	162.07	1145.21	319.94	0.19	6.43	4.38	10.39
Mukoni	2.52	71.10	5.64	40.20	305.96	127.75	0.08	1.94	1.65	2.40
Muzungu	6.86	159.71	14.62	99.84	711.54	340.54	0.37	2.90	5.44	7.81
Kihira	15.06	411.68	36.01	70.77	1368.97	245.06	0.42	7.49	1.80	2.73
Chabiringa	0.04	3.20	0.35	20.22	752.99	49.59	0.27	1.47	1.08	0.64
Kamutoni	0.03	3.20	0.41	11.55	406.14	20.36	0.14	0.84	0.67	0.35
Rwankwi	1.76	196.10	16.37	107.42	4696.05	776.76	0.87	4.92	27.62	24.89
Ndata	0.74	138.19	10.11	51.96	1726.19	277.44	0.30	1.85	12.07	9.85
Rangira	56.17	4206.60	379.14	7437.30	23689.23	3651.04	6.49	92.32	96.75	90.73
Ngwenda	56.47	1737.54	163.21	687.11	2516.19	518.14	0.52	17.58	8.67	13.53
Rwahambi	28.11	356.82	39.71	431.45	970.14	153.30	0.39	3.85	3.15	3.97
Virunga total	203.12	8860.42	781.94	9425.68	39547.22	6740.68	10.42	148.69	166.67	178.32

Kihira was sampled downstream of a confluence, one river is from the west in the Mitumba range (Figure 1) and the other from the east. During the last three sampling campaigns, the two tributaries of Kihira were also sampled, and the eastern was found to bring in O_2-deficient water, of high specific conductivity, TA, CH_4, and N_2O. Except for CH_4, these previous parameters (%O_2, TA, and N_2O) showed similar patterns as Chabiringa and Kamutoni. The eastern tributary collects inflowing water containing CH_4 produced in a small swamp (supporting information Figure S1), which could explain the elevated CH_4 found in Kihira. In contrast, the western tributary brought almost the entire TSM and POC load, as a consequence of its mountainous origin in the Mitumba range and its course along a clayey and steep catchment.

As mentioned above, most rivers were only small sources of N_2O to the atmosphere, as observed in other near-pristine tropical rivers with low NO_3^- and NH_4^+ [*Bouillon et al*., 2012; *Borges et al*., 2015] and unlike most nitrogen-enriched temperate rivers that have high N_2O concentrations [*Beaulieu et al*., 2010a, 2010b; *Baulch et al*., 2011]. The higher N_2O in Chabiringa, Kamutoni and Kihira were associated with high NO_3^- and low NO_2^- and O_2 (Figures 8c and 8d; respectively) that suggests active denitrification in the groundwaters. Such correlations between N_2O and NO_2^- were also observed in some temperate rivers [*Dong et al*., 2004].

The CH_4 concentration of Virunga rivers (4−5052 nmol L^{-1}) have a broader range than previous data from African rivers such as Comoé, Bia, and Tanoé rivers in West Africa (50–870 nmol L^{-1}) [*Koné et al*., 2010], Tana river in Kenya (50–500 nmol L^{-1}) [*Bouillon et al*., 2009], the Oubangui river in Central Africa (50–300 nmol L^{-1}) [*Bouillon et al*., 2012], but similar to the Athi-Galana-Sabaki rivers in Kenya (2–6729 μmol L^{-1}) [*Marwick et al*., 2014], although for the latter the highest values were related to organic matter inputs from the city of Nairobi. CH_4 of rivers of the VVP were also characterized by higher values than the adjacent Lake Kivu were CH_4 in surface waters varied from 18 to 197 nmol L^{-1} in the main basins of the lake and 89–303 in the Kabuno bay [*Borges et al*., 2011, 2012]. On the other hand, rivers of the VVP contain N_2O close to that observed in the Oubangui river [*Bouillon et al*., 2012] and the Athi-Galana-Sabaki rivers (18–198 nmol L^{-1}) [*Marwick et al*., 2014] but remain largely below concentrations normally found in temperate rivers where human activities have increased the DIN concentrations (see compilation by *Zhang et al*. [2010]).

4.5. Riverine Material Fluxes

Our estimated annual TSM, Si, NH_4^+, and SRP fluxes for Kihira (Table 3) are comparable with fluxes reported by *Muvundja et al*. [2009], except for the TP fluxes which were ∼90 times higher in their study compared to our estimate. For Chabiringa-Kamutoni, the TSM and SRP annual fluxes are similar for both studies, but our mean TP flux is 48 times higher, and our NH_4^+ flux is 23 times lower. In Mukoni-Muzungu, our TSM, Si, NH_4^+, and SRP fluxes are 18, 10, 12, and 8 times higher, respectively, while their mean TP flux is 4 times higher. The observed dissimilarities in fluxes between the two studies are due to differences already discussed among TSM and nutrients concentrations, and are even more pronounced due to differences in the annual discharges used. *Muvundja et al*. [2009] estimated their annual discharge using the float method described in *Harrelson et al*. [1994], which assumes a steady and uniform flow and does not offset flood and low flow conditions. For rivers of mountainous catchments (e.g., Kabuno bay), such a method results in discharges with errors of 30% or greater [*Bathurst*, 1990].

Table 4. Drainage Areas, Climatic Settings, Mean Solute Concentrations and Rates for Rivers in the Virunga Volcanic Province

	Drainage Area (km^2)	Runoff[d] (mm/year)	T (°C)	HCO_3^- (mmol/L)	TSM (mg/L)	TDS_{cat} (mg/L)	TDS_{cond} (mg/L)	CO_2 Consumption Rate (10^6 mol/km^2/year)	Si Weathering Rate (t/km^2/year)	Cationic Weathering Rate (t/km^2/year)	Chemical Weathering Rate (t/km^2/year)	Mechanical Weathering Rate (t/km^2/year)
Mubimbi[a]	55.7	1670	19.3	0.9	223.3	20.7	78.8	1.5	19.0	34.5	131.6	372.9
Kisheke[a]	5.8	1508	20.5	3.2	168.6	65.0	214.0	4.9	34.1	98.0	322.7	254.3
Renga[a]	43.6	1651	21.7	2.6	181.7	61.6	195.6	4.4	26.2	101.7	323.1	300.1
Mukoni[a]	15.4	1119	22.5	5.2	146.0	118.6	384.9	5.8	19.8	132.8	430.9	163.4
Muzungu[a]	16.1	2637	22.3	5.4	161.3	130.8	402.7	14.2	44.1	345.0	1062.0	425.5
Kihira[b]	31.7	1559	20.3	10.9	304.4	275.2	808.1	17.0	43.1	428.9	1259.5	474.5
Chabiringa[b]	8.5	3326	17.4	11.1	1.3	294.3	835.9	37.0	88.4	978.7	2779.9	4.3
Kamutoni[b]	10.2	1430	17.7	11.3	1.7	308.1	840.7	16.1	39.6	440.6	1202.4	2.5
Rwankwi[b]	95.0	1505	19.1	6.9	12.3	159.1	433.1	10.4	49.4	239.4	651.8	18.5
Ndata[b]	70.5	829	19.4	6.7	12.7	149.6	398.0	5.6	24.5	124.0	329.8	10.5
Rangira[a]	1351.0	1313	20.4	4.0	31.7	83.5	250.3	5.2	17.5	109.6	328.7	41.6
Ngwenda[c]	231.8	1297	22.0	0.3	187.7	6.1	30.1	0.4	10.9	7.9	39.0	243.6
Rwahambi[c]	107.3	1120	21.6	0.6	233.8	16.6	55.5	0.7	9.0	18.6	62.1	261.9

[a]Rivers draining basaltic formations.
[b]Rivers draining acid metamorphic rock formations.
[c]Rivers draining lacustrine formations.
[d]Estimated runoff.

The estimated mean TSM (198.0 t km^{-2} yr^{-1}) and POC (7.43 t km^{-2} yr^{-1}) yields of VVP rivers were much higher when compared to those of the Congo River (8.8 t km^{-2} yr^{-1} for TSM and 0.6 t km^{-2} yr^{-1} for POC) [*Coynel et al*., 2005], the Oubangui River (4.8–5.1 t km^{-2} yr^{-1} for TSM and ~0.3 t km^{-2} yr^{-1} for POC) [*Coynel et al*., 2005; *Bouillon et al*., 2012], and the world largest rivers (see compilation by *Meybeck* [1982], *Spitzy and Leenheer* [1991], and *Coynel et al*. [2005]). The estimated mean DOC yields (3.11 t km^{-2} yr^{-1}) were similar to that of the Congo River (3.5 t km^{-2} yr^{-1}) [*Coynel et al*., 2005], but higher compared to the Oubangui River (1.1–1.4 t km^{-2} yr^{-1}) [*Coynel et al*., 2005; *Bouillon et al*., 2012].

The estimated DOC (0.74–6.19 t km^{-2} yr^{-1}) and POC (0.31–21.08 t km^{-2} yr^{-1}) yields in the VVP were almost in the same range with those reported for Guadeloupan volcanic islands [1.9–8.9 t km^{-2} yr^{-1} and 8.1–25.5 t km^{-2} yr^{-1}, respectively, for DOC and POC) [*Lloret et al*., 2011, 2013]. This could partly be explained by two major similarities between the areas. First, both fields experience tropical wet season, and second; their organic C soil content are similar: 1–25% for Virunga and 10–15% for Guadeloupe [*Lloret*, 2010].

4.6. Weathering and Atmospheric CO_2 Consumption Rates

The discharge-weighted mean TDS_{cat}, TDS_{cond}, and TSM yielded cationic weathering rates from 7.9 to 978.7 t km^{-2} yr^{-1}, chemical weathering rates from 39.0 to 2779.9 t km^{-2} yr^{-1}, and mechanical weathering rates between 2.5 and 474.5 t km^{-2} yr^{-1} (Table 4). The Si weathering rates and CO_2 consumption rates ranged from 9.0 to 88.4 t km^{-2} yr^{-1}, and 0.4 × 10^6 to 37.0 × 10^6 mol km^{-2} yr^{-1}, respectively. Chemical weathering was more important in rivers draining basaltic fields, whereas mechanical weathering was prevailing in others lithological formations; i.e., acid metamorphic and lacustrine (Table 4). An opposite trend, with higher mechanical than chemical weathering rates, has been observed in the tropical basaltic field of Réunion, [*Louvat and Allègre*, 1997]. The large influence of lithology on the chemical weathering and CO_2 consumption rates in the Virunga is evident, and illustrated, for example, by comparing Chabiringa (basaltic terrain) with Ngwenda (lacustrine terrain). Thus, Chabiringa (drainage area of 8.5 km^2) showed the highest weathering (Si, cationic, and chemical) and CO_2 consumption rates; whereas Ngwenda (231.8 km^2 drainage area) showed the lowest. Similar trends are observed when comparing rivers draining basaltic terrain (i.e., Kihira, Chabiringa, Kamutoni, Rwankwi, and Ndata) with those of lacustrine and metamorphic rocks. As a result, the five rivers of basaltic terrain cover only 10.6% of the total studied drainage area, but are responsible for 23.4% of the total CO_2 consumed, 22.6% of the total Si weathered, and 25.8% of the total major cations weathered. Basalt was characterized by a mean chemical weathering rate and mean CO_2 consumption rate 2.87 and 2.88 times higher, respectively, compared to values in acid metamorphic rocks terrain; and 24.6 and 32.7 times higher than in lacustrine terrain.

Chemical weathering rates were found to depend strongly on runoff, since there were strong linear relationships between runoff and CO_2 consumption rates ($r^2 = 0.63$; Figure 9a), cationic weathering rates ($r^2 = 0.62$; Figure 9b), and Si weathering rates ($r^2 = 0.66$; Figure 9c). In contrast, no positive temperature dependency

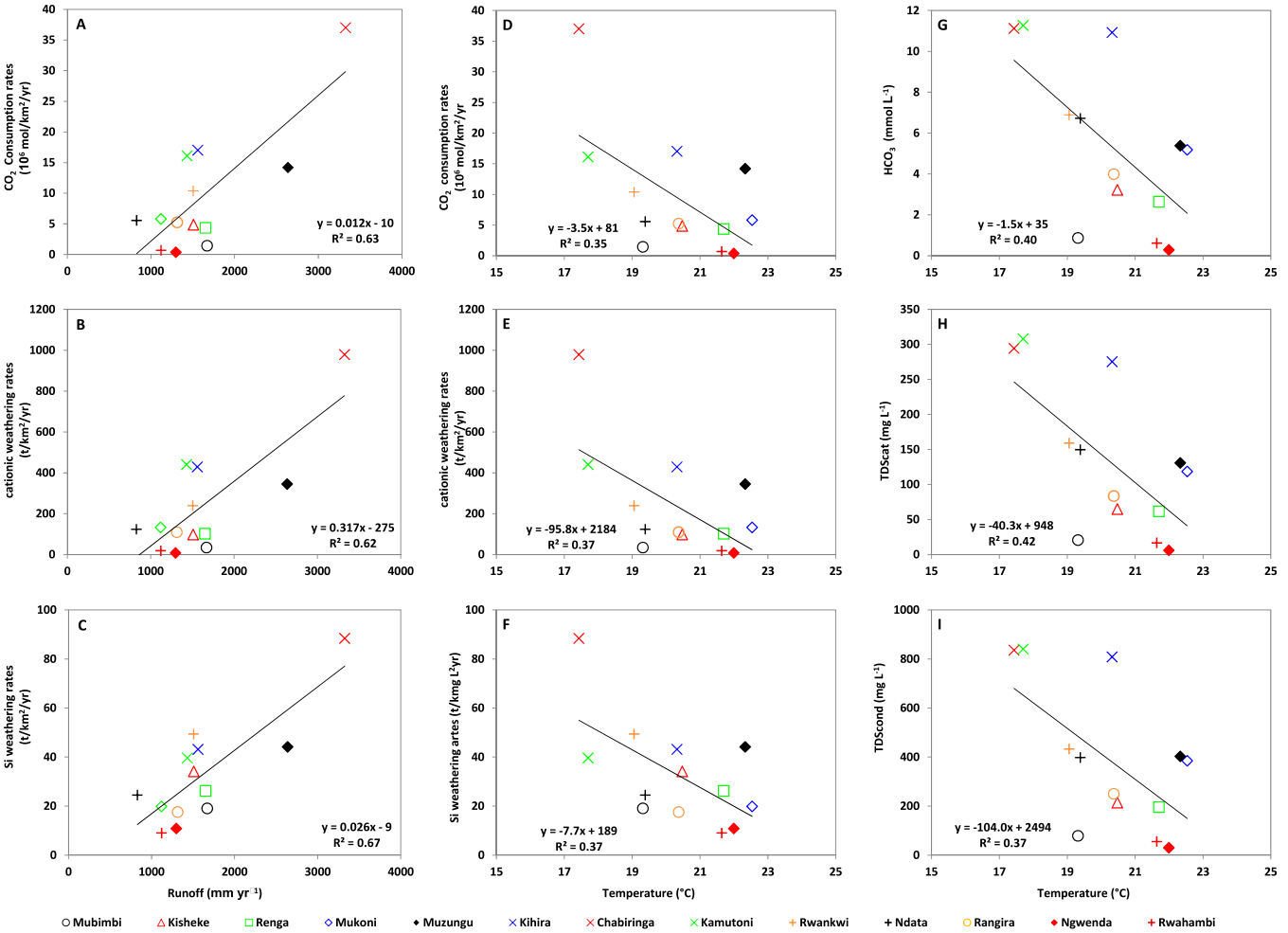

Figure 9. (a-c) Mean riverine CO_2 consumption rates, cationic weathering rates, and Si weathering rates versus runoff; (d-f) mean riverine CO_2 consumption rates, cationic weathering rates and Si weathering rates versus temperature; and (g-i) mean HCO_3^-, TDScat, TDScond concentrations versus corresponding mean water temperature.

was found for either the CO_2 consumption rate (Figure 9d), cationic weathering rate (Figure 9e), and Si weathering rate (Figure 9f). In addition, no dependency on temperature was found for elements released during chemical weathering (Figures 9h and 9i), or for the HCO_3^- ions which balance the major cation charge (Figure 9g), as previously noted by *Amiotte-Suchet and Probst* [1995] and *Bluth and Kump* [1994] in the French basaltic basins. *Dessert et al.* [2003] attributed this pattern to the relative similarity among temperatures of neighboring watersheds, and thus only the effect of runoff could be observed.

The mean CO_2 consumption rate estimated for the study area (9.46×10^6 mol km^{-2} yr^{-1}, or 1.72×10^7 mol km^{-2} yr^{-1} if only considering the basaltic fields is markedly higher than data reported in the literature for other tropical basaltic regions (Figure 10). On the other hand, the measured mean atmospheric C yield (113.68 t C km^{-2} yr^{-1}) is much higher than previous model estimates for the Virunga (0.5–5 t C km^{-2} yr^{-1}) [*Hartmann et al.*, 2009]. Since the Virunga mean CO_2 consumption rate is >10 times the global average (1.99 t C km^{-2} yr^{-1}) [*Hartmann et al.*, 2009], the VVP can thereby be considered as CO_2 consumption "hot spot zone" according to a classification by *Meybeck et al.* [2006].

Factors contributing to the high CO_2 consumption rates in the VVP include the high chemical weathering rate of volcanic rocks [*Dessert et al.*, 2001], the high reactivity of basaltic glasses and minerals [*Berner and Berner*, 1996; *Oelkers and Gislason*, 2001; *Gislason and Oelkers*, 2003], and the high annual mean runoff (1613 mm yr^{-1}) and temperature (20.3°C).

Furthermore, the CO_2 consumption rates that can be calculated with the model of *Dessert et al.* [2003] based on a compilation of data in other basalt dominated areas are lower than those we computed (Figure 11).

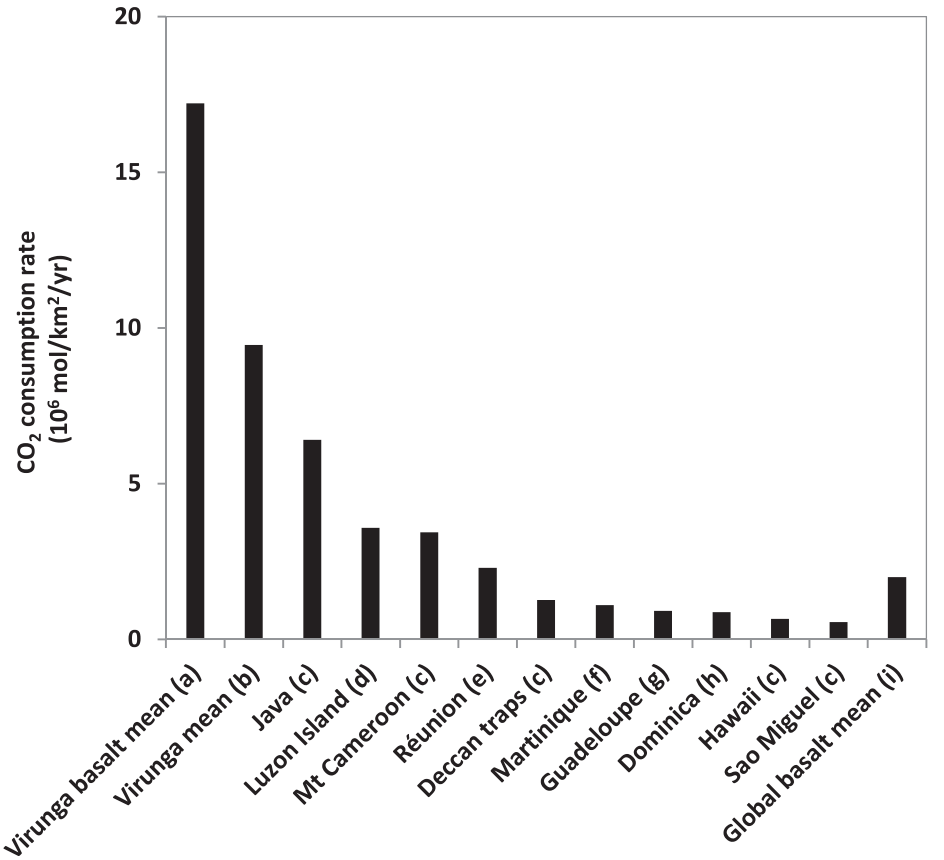

Figure 10. Comparison of Virunga basalt mean and Virunga mean CO_2 consumption rates with the rates of other tropical basaltic provinces, and the Caribbean basalt-andesite formations. (a) represents the mean CO_2 consumption rate for the rivers draining Virunga basalt, (b) the mean CO_2 consumption rate for the whole Virunga, i.e., basalt, metamorphic rocks and lacustrine; (c) is from *Dessert et al*. [2003], (d) *Schopka et al*. [2011], (e) *Louvat and Allègre* [1997], (f) *Rad et al*. [2006], (g) *Lloret et al*. [2011], (h) *Goldsmith et al*. [2010], and (i) is from *Louvat* [1997].

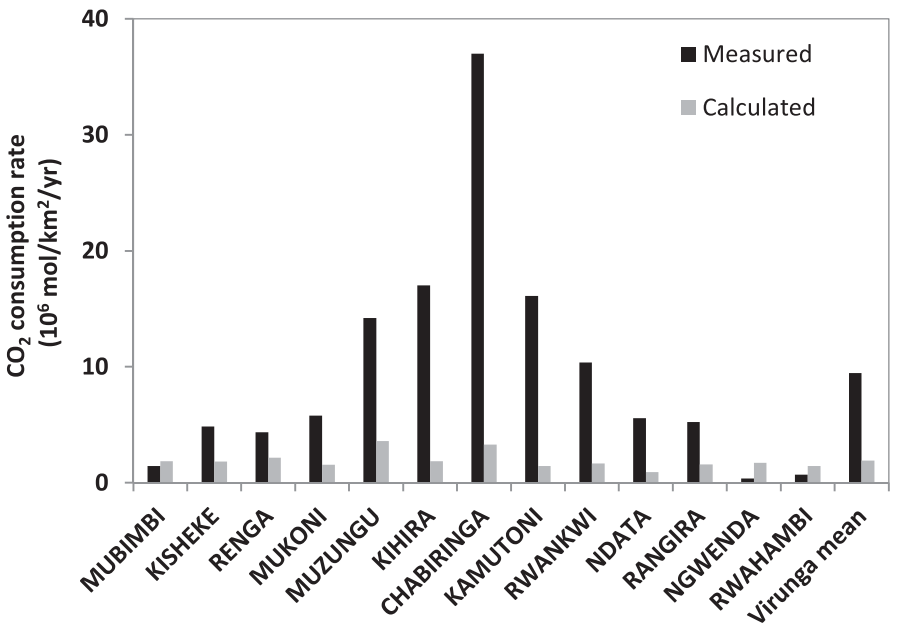

Figure 11. Comparison between the CO_2 consumption rates from field data (measured) and calculated CO_2 consumption (calculated) rates applying the regression model as a function of runoff and temperature as suggested by *Dessert et al*. [2003].

This is indicative of the high solubility of the rocks in the watershed which is probably related to the fact that the VVP is a young active tectonic and volcanic area.

5. Conclusions

The present study offers the first geochemical data set from an under-documented area, in terms of river GHGs and major cations concentrations, DOC, POC, and DIC concentrations and their respective $\delta^{13}C$ signatures, chemical weathering rates, and atmospheric CO_2 consumption rates. The VVP is a tropical, young active tectonic and volcanic area, relatively undisturbed by anthropogenic activities.

Our results showed that soil, land use, and morphology control the spatial distribution of riverine organic matter (POC and DOC concentrations and origin), TSM, and nutrient concentrations. The DIC was found to largely dominate the C pool. Intense soil erosion leads to high TSM yields in the mountainous rivers draining into Kabuno bay. Lithology and volcanism exert a strong control on the major cation and DIC concentrations, and their spatial distribution. Thus, high basalt (and secondary soil) chemical weathering and leaching mediated by magmatic CO_2 inputs yielded markedly high Na^+, K^+, Mg^{2+}, and Si; particularly in basaltic fields. CH_4 concentrations were consistently above atmospheric equilibrium, and thus Virunga rivers were sources of CH_4 to the atmosphere. In contrast, only a few rivers were a net source of N_2O to the atmosphere, as denitrification in groundwaters depleted N_2O concentrations below their atmospheric equilibrium levels in other rivers.

The multilithological state of the VVP highlights the strong influence of lithology on the chemical weathering rates, and the associated atmospheric CO_2 consumption rate under the same climatic conditions. In fact, we noticed that the mean chemical weathering rate and mean CO_2 consumption rate in basalt terrain were respectively ~3 higher compared to values in acid metamorphic rocks terrain; and ~25 and ~33 higher compared to lacustrine terrain. Our study additionally showed that runoff and lithology are the main factors controlling the rates of local chemical weathering and atmospheric CO_2 consumption rates. The $\delta^{13}C$-DIC data indicate that part of the CO_2 involved in chemical weathering is geogenic, and thus the active volcanism may partly explain the higher CO_2 consumption and weathering rates reported in this study compared to the literature data.

Note that much of the Virunga lava field is not drained by rivers. This zone is composed of macroporous materials, slightly fractured, and therefore considerably permeable. Rainfall is influenced by the Nyiragongo and Nyamulagira emissions and pH values as low as three have been recorded [*Cuoco et al*., 2012a, 2012b]. The precipitation interacts with surface and deep basalts, but the resulting atmospheric CO_2 consumption rate is not included in the data we report.

Acknowledgments

We are grateful to Stephane Hoornaert, Marc-Vincent Commarieu and Sandro Petrovic (Université de Liège), and Zita Kelemen (KU Leuven) for their support during sample analysis, Trent Marwick and Cristian Teodoru (KU Leuven) for help and advice with the GIS analysis, Jens Hartmann for kindly providing access to the GLIM database, Marcellin Kasereka for help in field sampling, and Bernhard Peucker-Ehrenbrink (reviewer) and two additional anonymous reviewers for constructive comments on a previous version of the manuscript. This work was funded by the European Research Council starting grant project AFRIVAL (African river basins: Catchment-scale carbon fluxes and transformations, StG 240002) and the Belgian Federal Science Policy Office EAGLES (East African Great Lake Ecosystem Sensitivity to changes, SD/AR/02A) projects. AVB is a senior research associate at the FRS-FNRS. The full data set is provided as supporting information (SI) (Balagizial-ds01 and Balagizial-ds02; XLS).

References

American Public Health Association (1998), *Standard Methods for the Examination of Water and Wastewater*, 20th ed., Washington, D. C.

Amiotte-Suchet, P., and J. L. Probst (1995), A global model for present-day atmospheric/soil CO_2 consumption by chemical erosion of continental rocks (GEM-CO_2), *Tellus, Ser. A*, *47*, 273–280.

Amiotte-Suchet, P., J. L. Probst, and W. Ludwig (2003), Worldwide distribution of continental rock lithology: Implications for the atmospheric/soil CO_2 uptake by continental weathering and alkalinity river transport to the oceans, *Global Biogeochem. Cycles*, *17*(2), 1038, doi:10.1029/2002GB001891.

Andersen, T., A. E. Marlina, and E. Muriel (2012), Petrology of combeite- and götzenite-bearing nephelinite at Nyiragongo, Virunga Volcanic Province in the East African Rift, *Lithos*, *152*, 105–121, doi:10.1016/j.lithos.2012.04.018.

Andersen, T., A. E. Marlina, and E. Muriel (2014), Extreme peralkalinity in delhayelite- and andremeyerite-bearing nephelinite from Nyiragongo volcano, East African Rift, *Lithos*, *206–207*, 164–178, doi:10.1016/j.lithos.2014.07.025.

Aoki, K., and H. Kurasawa (1984), Sr isotope study of the tephrite series from Nyamuragira volcano, Zaire, *Geochem. J.*, *18*, 95–100.

Aoki, K., T. Yoshida, K. Yusa, and Y. Nakamura (1985), Petrology and geochemistry of the Nyamuragira volcano, Zaire, *J. Volcanol. Geotherm. Res.*, *25*, 1–28.

Atekwana, E. A., E. A. Atekwana, R. S. Rowe, D. D. Werkema Jr., and F. D. Legall (2004), the relationship of total dissolved solids measurements to bulk electrical conductivity in an aquifer contaminated with hydrocarbon, *J. Appl. Geophys.*, *56*, 281–294, doi:10.1016/j.jappgeo.2004.08.003.

Baccini, A., N. Laporte, S. J. Goetz, M. Sun, and H. Dong (2008), A first map of tropical Africa's above-ground biomass derived from satellite imagery, *Environ. Res. Lett.*, *3*, 045011, doi:10.1088/1748-9326/3/4/045011.

Bastviken, D., L. J. Tranvik, J. A. Downing, P. M. Crill, and A. E. Prast (2011), Freshwater methane emissions offset the continental carbon sink, *Science*, *331*, 50, doi:10.1126/science.1196808.

Bathurst, J. C. (1990), Tests of three discharge gauging techniques in mountain rivers, in *Hydrology of Mountainous Areas*, IAHS Publ. no 190, pp. 93–100, Wallingford, U. K.

Batjes, N. H. (2008), Mapping soil carbon stocks of Central Africa using SOTER, *Geoderma*, *146*, 58–65, doi:10.1016/j.geoderma.2008.05.006.

Baulch, H. M., S. L. Schiff, R. Maranger, and P. J. Dillon (2011), Nitrogen enrichment and the emission of nitrous oxide from streams, *Global Biogeochem. Cycles*, *25*, GB4013, doi:10.1029/2011GB004047.

Beaulieu, J. J., et al. (2010a), Nitrous oxide emission from denitrification in stream and river networks, *Proc. Natl. Acad. Sci. U. S. A.*, *108*, 214–219, doi:10.1073/pnas.1011464108.

Beaulieu, J. J., W. D. Huster, and J. A. Rebholz (2010b), Nitrous oxide emissions from a large, impounded river: The Ohio River, *Environ. Sci. Technol.*, *44*(19), 7527–7533, doi:10.1021/es1016735.

Beck, V., et al. (2012), Methane airborne measurements and comparison to global models during BARCA, *J. Geophys. Res.*, *117*, D15310, doi:10.1029/2011JD017345.

BEGo (Synoptics, Keyobs, Royal Museum for Central Africa, Catholic University of Louvain) (2005), Parc National des Virunga, République Démocratique du Congo, 1/260,000, Map realized in the framework of the BEGo (Building Environment for the Gorilla's) project, co-financed by ESA and UNESCO-WHC, Belgium.

Berner, E. K., and R. A. Berner (1996), *Global Environment: Water, Air, and Geochemical Cycles*, Prentice-Hall, N. J.

Bluth, G. J. S., and L. R. Kump (1994), Lithologic and climatologic controls of river chemistry, *Geochim. Cosmochim. Acta*, *58*, 2341–2359.

Borges, A. V., G. Abril, B. Delille, J.-P. Descy, and F. Darchambeau (2011), Diffusive methane emissions to the atmosphere from Lake Kivu (Eastern Africa), *J. Geophys. Res.*, *116*, G03032, doi:10.1029/2011JG001673.

Borges, A. V., et al. (2012), Variability of carbon dioxide and methane in the Epilimnion of Lake Kivu, in *Lake Kivu: Limnology and Biogeochemistry of a Tropical Great Lake, Aquat. Ecol.*, vol. 5, edited by J. P. Descy, pp. 47–66, Springer, Dordrecht, Netherlands, doi:10.1007/978-94-007-4243-7_4.

Borges, A. V., et al. (2015), Globally significant greenhouse gas emissions from African inland waters, *Nat. Geosci.*, doi:10.1038/NGEO2486.

Bouillon, S., et al. (2009), Distribution, origin and cycling of carbon in the Tana River (Kenya): A dry season basin-scale survey from headwaters to the delta, *Biogeosciences*, *6*, 2475–2493, doi:10.5194/bg-6-2475-2009.

Bouillon, S., A. Yambélé, R. G. M. Spencer, D. P. Gillikin, P. J. Hernes, J. J. Six, R. Merckx, and A. V. Borges (2012), Organic matter sources, fluxes and greenhouse gas exchange in the Oubangui River (Congo River basin), *Biogeosciences*, *9*, 2045–2062, doi:10.5194/bg-9-2045-2012.

Bouillon, S., A. Yambélé, D. P. Gillikin, C. Teodoru, F. Darchambeau, T. Lambert, and A. V. Borges (2014), Contrasting biogeochemical characteristics of right-bank tributaries and a comparison with the mainstem Oubangui River, Central African Republic (Congo River basin), *Sci. Rep.*, *4*, 5402, doi:10.1038/srep05402.

Bousquet, P., et al. (2011), Source attribution of the changes in atmospheric methane for 2006–2008 *Atmos. Chem. Phys.*, *11*, 3689–3700, doi:10.5194/acp-11-3689-2011.

Chakrabarti R., A. R. Basu, A. P. Santo, D. Tedesco, and O. Vaselli (2009), Isotopic and geochemical evidence for a heterogeneous mantle plume origin of the Virunga volcanics, Western rift, East African Rift system, *Chem. Geol.*, *259*, 273–289, doi:10.1016/j.chemgeo.2008.11.010.

Coynel, A., P. Seyler, H. Etcheber, M. Meybeck and D. Orange (2005), Spatial and seasonal dynamics of total suspended sediment and organic carbon species in the Congo River, *Global Biogeochem. Cycles*, *19*, GB4019, doi:10.1029/2004GB002335.

Cuoco, E., A. Spagnuolo, C. Balagizi, S. Francesco, F. Tassi, O. Vaselli, and D. Tedesco (2012a), Impact of volcanic emissions on rainwater chemistry: The case of Mt. Nyiragongo in the Virunga volcanic region DRC), *J. Geochem. Explor.*, *125*, 69–79, doi:10.1016/j.gexplo.2012.11.008.

Cuoco, E., D. Tedesco, R. J. Poreda, J. C. Williams, S. De Francesco, C. Balagizi, and T. H. Darrah (2012b), Impact of volcanic plume emissions on rain water chemistry during the January 2010 Nyamuragira eruptive event: Implications for essential potable water resources, *J. Hazard. Mater.*, *244–245*, 570–581, doi:10.1016/j.jhazmat.2012.10.055.

Deines, P. (2002), The carbon isotope geochemistry of mantle xenoliths, *Earth Sci. Rev.*, *58*, 247–278, doi:10.1016/S0012-8252(02)00064-8.

Demant, A., P. Lestrade, T. R. Lubala, A. B. Kampunzu, and J. Durieux (1994), Volcanological and petrological evolution of Nyiragongo volcano, Virunga volcanic field, Zaire, *Bull. Volcanol.*, *56*, 47–61.

Denaeyer, M. E. (1972), Les laves du fossé tectonique de l'Afrique Centrale. II: Magmatologie, *Ann. Musée R. Afrique Cent.*, *72*, 250.

Denaeyer, M. E. (1975), *Le glacis des volcans actifs au nord du Lac Kivu (république du Zaïre), Ed. du Museum, Sér. C*, Sci. de la terre, Paris.

Dessert, C., B. Dupré, L. M. François, J. Schott, J. Gaillardet, G. Chakrapani and S. Bajpai (2003), Erosion of Deccan Traps determined by river geochemistry, impact on the global climate and the $^{87}Sr/^{86}Sr$ ratio of seawater, *Earth Planet. Sci. Lett.*, *188*, 459–474.

Dessert, C., B. Dupre, J. Gaillardet, L. M. Francois, and C. J. Allègre (2003), Basalt weathering laws and the impact of basalt weathering on the global carbon cycle, *Chem. Geol.*, *202*, 257–273, doi:10.1016/j.chemgeo.2002.10.001.

Document stratégique de réduction de la pauvreté (2005), *Province du Nord-Kivu*, SRP-Nord-Kivu, Goma, RD Congo.

Dong, L. F., D. B. Nedwell, I. Colbeck, and J. Finch (2004), Nitrous oxide emission from some English and Welsh rivers and estuaries, *Water Air Soil Pollut.*, *4*(6), 127–134, doi:10.1007/s11267-005-3022-z.

Ehleringer, J. R. (1991), $^{13}C/^{12}C$ Fractionation and its utility in terrestrial plant studies, in *Carbon Isotope Techniques*, edited by B. Fry, pp. 187–200, Academic, N. Y.

Farr, T. G., et al. (2007), The shuttle radar topography mission, *Rev. Geophys.*, *45*, RG2004, doi:10.1029/2005RG000183.

Fraser, A., et al. (2013), Estimating regional methane surface fluxes: The relative importance of surface and GOSAT mole fraction measurements, *Atmos. Chem. Phys.*, *13*, 5697–5713, doi:10.5194/acp-13-5697-2013.

Gaillardet, J., B. Dupré, P. Louvat, and C. J. Allègre (1999), Global silicate weathering and CO_2 consumption rates deduced from the chemistry of large rivers, *Chem. Geol.*, *159*(1–4), 3–30.

Gillikin, D. P., and S. Bouillon (2007), Determination of $\delta^{18}O$ of water and $\delta^{13}C$ of dissolved inorganic carbon using a simple modification of an elemental analyzer-isotope ratio mass spectrometer (EA-IRMS): An evaluation, *Rapid Commun. Mass Spectrom.*, *21*, 1475–1478, doi:10.1002/rcm.2968.

Gislason, S. R., and E. H. Oelkers (2003), Mechanism, rates and consequences of basaltic glass dissolution. II: An experimental study of the dissolution rates of basaltic glass as a function of pH and temperature, *Geochim. Cosmochim. Acta*, *67*, 3817–3832, doi:10.1016/S0016-7037(03)00176-5.

Global Land Cover 2000 database (2003), *European Commission*, Joint Res. Cent. [Available at http://bioval.jrc.ec.europa.eu/products/glc2000/glc2000.php, last accessed 20 Jan. 2015.]

Goldsmith, S. T., A. E. Carey, B. M. Johnson, S. A. Welch, W. B. Lyons, W. H. McDowell, and J. S. Pigott (2010), Stream geochemistry, chemical weathering and CO_2 consumption potential of andesitic terrains, Dominica, Lesser Antilles, *Geochim. Cosmochim. Acta*, *74*, 85–103, doi:10.1016/j.gca.2009.10.009.

Guibert, P. (1978), Contribution à l'étude du volcanisme de la chaîne des Virunga (République du Zaïre): Le volcan Mikeno, PhD thesis, Univ. de Genève, Geneva, Switzerland.

Harrelson, C. C., C. L. Rawlins, and J. P. Potyondy (1994), Stream channel reference sites: An illustrated guide to field technique, *Gen. Tech. Rep. RM-245*, 61 pp., Dep. of Agric., For. Serv., Rocky Mt. For. and Range Exp. Stn., Fort Collins, Colo.

Hartmann, J., and N. Moosdorf (2011), Chemical weathering rates of silicate-dominated lithological classes and associated liberation rates of phosphorus on the Japanese Archipelago-Implications for global scale analysis, *Chem. Geol.*, *287*, 125–157, doi:10.1016/j.chemgeo.2010.12.004.

Hartmann, J., and N. Moosdorf (2012), The new global lithological map database GLiM: A representation of rock properties at the Earth surface, *Geochem. Geophys. Geosyst.*, *13*, Q12004, doi:10.1029/2012GC004370.
Hartmann, J., N. Jansen, H. H. Dürr, S. Kempe, and P. Köhler (2009), Global CO_2-consumption by chemical weathering: What is the contribution of highly active weathering regions?, *Global Planet. Change*, *69*, 185–194, doi:10.1016/j.gloplacha.2009.07.007.
Hartmann, J., N. Moosdorf, R. Lauerwald, M. Hinderer, and A. J. West (2014), Global chemical weathering and associated P-release—The role of lithology, temperature and soil properties, *Chem. Geol.*, *363*, 145–163, doi:10.1016/j.chemgeo.2013.10.025.
Head, E. M., A. M. Shaw, P. J. Wallace, K. W. W. Sims, and S. A. Carn (2011), Insight into volatile behavior at Nyamuragira volcano (D.R. Congo, Africa) through olivine-hosted melt inclusions, *Geochem. Geophys. Geosyst.*, *12*, Q0AB11, doi:10.1029/2011GC003699.
Hertogen, J., L. Vanlerberghe, and M. R. Namegabe (1985), Geochemical evolution of the Nyiragongo volcano (Virunga, Western African Rift, Zaire), *Bull. Geol. Soc.*, *57*(1–2), 21–35.
Hijmans, R. J., S. E. Cameron, J. L. Parra, P. G. Jones, and A. Jarvis (2005), Very high resolution interpolated climate surfaces for global land areas, *Int. J. Climatol.*, *25*, 1965–1978, doi:10.1002/joc.1276.
Ittekkot, V., and R. W. P. M. Laane (1991), Fate of riverine particulate organic matter, in *Biogeochemistry of Major World Rivers*, edited by E. T. Degens, S. Kempe, and J. E. Richey, chap. 6, pp. 233–243, John Wiley, N. Y.
Julley, D. W., M. Windowson, and S. Self (2008), Volcanogenic nutrient fluxes and plant ecosystems in large igneous provinces: An example from the Columbia River Basalt Group, *J. Geol. Soc.*, *165*, 955–966, doi:10.1144/0016-76492006-199.
Kirschke, S., et al. (2013), Three decades of global methane sources and sinks, *Nat. Geosci.*, *6*, 813–823, doi:10.1038/NGEO1955.
Koné, Y. J. M., G. Abril, B. Delille, and A. V. Borges (2010), Seasonal variability of methane in the rivers and lagoons of Ivory Coast (West Africa), *Biogeochemistry*, *100*, 21–37, doi:10.1007/s10533-009-9402-0.
Lauerwald, R., G. G. Laruelle, J. Hartmann, P. Ciais, and P. A. G. Regnier (2015), Spatial patterns in CO_2 evasion from the global river network, *Global Biogeochem. Cycles*, *29*, 534–554, doi:10.1002/2014GB004941.
Le Quéré, C., et al. (2014), Global carbon budget 2014, *Earth Syst. Sci. Data Discuss.*, *7*, 521–610, doi:10.5194/essdd-7-521-2014.
Lloret, E. (2010), Dynamique du carbone dans des petits bassins versants tropicaux, exemple de la Guadeloupe, PhD thesis, Univ. of Paris, Paris.
Lloret, E., C. Dessert, J. Gaillardet, P. Albéric, O. Crispi, C. Chaduteau, and M. F. Benedetti (2011), Comparison of dissolved inorganic and organic carbon yields and fluxes in the watersheds of tropical volcanic islands, examples from Guadeloupe, *Chem. Geol.*, *280*, 65–78, doi:10.1016/j.chemgeo.2010.10.016.
Lloret, E., C. Dessert, L. Pastor, E. Lajeunesse, O. Crispi, J. Gaillardet, and M. F. Benedetti (2013), Dynamic of particulate and dissolved organic carbon in small volcanic mountainous tropical watersheds, *Chem. Geol.*, *351*, 229–244, doi:10.1016/j.chemgeo.2013.05.023.
Louvat, P. (1997), Etude géochimique de l'érosion fluviale d'îles volcaniques à l'aide des bilans d'éléments majeurs et traces, PhD thesis, 322 pp., Univ. of Paris, Paris.
Louvat, P., and C. J. Allègre (1997), Present denudation rates at Réunion Island determined by river geochemistry: Basalt weathering and mass budget between chemical and mechanical erosions, *Geochim. Cosmochim. Acta*, *61*, 3645–3669.
Ludwig, W., J. L. Probst, and S. Kempe (1996), Predicting the oceanic input of organic carbon by continental erosion, *Global Biogeochem. Cycles*, *10*(1), 23–41, doi:10.1029/95GB02925.
Mann, P. J., et al. (2014), The biogeochemistry of carbon across a gradient of streams and rivers within the Congo Basin, *J. Geophys. Res. Biogeosci.*, *119*, 687–702, doi:10.1002/2013JG002442.
Marcelot, G., C. Dupuy, J. Dostal, J. P. Rancon, and A. Pouclet (1989), Geochemistry of mafic volcanic rocks from Lake Kivu (Zaire and Rwanda) section of the Western Branch of the African Rift, *J. Volcanol. Geotherm. Res.*, *39*, 73–88.
Mariotti, A., F. Gadel, P. Giresse, and Kinga-Mouzeo (1991), Carbon isotope composition and geochemistry of particulate organic matter in the Congo River (Central Africa): Application to the study of Quaternary sediments off the mouth of the river, *Chem. Geol.*, *86*, 345–357.
Martins, O., and J. L. Probst (1991), Biogeochemistry of major African Rivers: Carbon and mineral transport, in *Biogeochemistry of Major World Rivers*, edited by E. T. Degens, S. Kempe, and J. E. Richey, chap. 6, pp. 129–155, John Wiley, N. Y.
Marwick, T. R., F. Tamooh, B. Ogwoka, C. Teodoru, A. V. Borges, F. Darchambeau, and S. Bouillon (2014), Dynamic seasonal nitrogen cycling in response to anthropogenic N loading in a tropical catchment, Athi-Galana-Sabaki River, Kenya, *Biogeosciences*, *11*, 1–18, doi:10.5194/bg-11-1-2014.
Mayaux, P., E. Bartholomé, S. Fritz, and A. Belward (2004), A new land-cover map of Africa for the year 2000, *J. Biogeogr.*, *31*, 861–877, doi:10.1111/j.1365-2699.2004.01073.x.
Meybeck, M. (1982), Carbon, nitrogen and phosphorus transport by world rivers, *Am. J. Sci.*, *282*, 401–450.
Meybeck, M. (1987), Global chemical weathering of surficial rocks estimated from river dissolved loads, *Am. J. Sci.*, *287*, 401–428.
Meybeck, M. (1993a), Natural sources of C, N, P and S, in *Interactions of C, N, P and S Biogeochemical Cycles and Global Change*, edited by R. Wollast, F. T. Mackenzie, and L. Chou, pp. 163–193, Springer, Berlin.
Meybeck, M. (1993b), Riverine transport of atmospheric carbon: Sources, global typology and budget, *Water Air Soil Pollut.*, *70*, 443–464.
Meybeck, M. (2005), Origins and behaviours of carbon species in World rivers, in *Erosion and Carbon Dynamics, Adv. Soil Sci.*, edited by E. Roose and R. Lal, pp. 209–238, CRC Press, Boca Raton, Fla.
Meybeck, M., H. H. Dürr and C. J. Vörösmarty (2006), Global coastal segmentation and its river catchment contributors: A new look at land-ocean linkage, *Glob. Biogeochem. Cycles*, *20*, GB1S90, doi:10.1029/2005GB002540.
Moon, S., C. P. Chamberlain, and G. E. Hilley (2014), New estimates of silicate weathering rates and their uncertainties in global rivers, *Geochim. Cosmochim. Acta*, *134*, 257–274, doi:10.1016/j.gca.2014.02.033.
Morimoto, N. (1989), Nomenclature of pyroxenes, *Can. Mineral.*, *27*, 143–156.
Munhoven, G. (2002), Glacial-interglacial changes of continental weathering: Estimates of the related CO_2 and HCO_3-flux variations and their uncertainties, *Global Planet. Change*, *33*(1–2), 155–176.
Muvundja, A. F., et al. (2009), Balancing nutrient inputs to Lake Kivu, *J. Great Lakes Res.*, *35*(3), 406–418, doi:10.1016/j.jglr.2009.06.002.
Oelkers, E. H., and S. R. Gislason (2001), The mechanism, rates and consequences of basaltic glass dissolution. I: An experimental study of the dissolution rates of basaltic glass as function of aqueous Al, Si and oxalic acid concentration at 25°C and pH = 3 and 11, *Geochim. Cosmochim. Acta*, *65*, 3671–3681.
Platz, T. (2002), Nyiragongo volcano, DR Congo-mineral chemistry and petrology, PhD thesis, Univ. of Greifswald, Inst. of Geol. Sci., Greifswald, Germany.
Pison, I., P. Bousquet, F. Chevallier, S. Szopa, and D. Hauglustaine (2009), Multi-species inversion of CH_4, CO and H_2 emissions from surface measurements, *Atmos. Chem. Phys.*, *9*, 5281–5297, doi:10.5194/acp-9-5281-2009.

Platz, T., S. F. Foley, and L. Andre (2004), Low-pressure fractionation of the Nyiragongo volcanic rocks, Virunga Province, D.R. Congo, *J. Volcanol. Geotherm. Res.*, *136*, 269–295, doi:10.1016/j.jvolgeores.2004.05.020.

Pouclet, A. (1974), Pétrographie du Rugarama, dernier cône adventif du volcan Nyamuragira (1971), (Rift W.-Africain), *Publ. Spéc.*, 1–28.

Pouclet, A. (1977), Contribution à l'étude structurale de l'aire volcanique des Virunga, rift de l'Afrique Centrale, *Rev. Géogr. Phys. Géol. Dyn.*, *19*(2), 115–124.

Rad, S., P. Louvat, C. Gorge, J. Gaillardet, and C. J. Allègre (2006), River dissolved and solid loads in the Lesser Antilles: New insight into basalt weathering processes, *J. Geochem. Explor.*, *88*, 308–312, doi:10.1016/j.gexplo.2005.08.063.

Ralison, O., F. Dehairs, J. J. Middelburg, A. V. Borges, and S. Bouillon (2008), Carbon biogeochemistry in the Betsiboka estuary (northwestern Madagascar), *Org. Geochem.*, *39*, 1649–1658, doi:10.1016/j.orggeochem.2008.01.010.

Raymond, P. A., et al. (2013), Global carbon dioxide emissions from inland waters, *Nature*, *503*, 355–359, doi:10.1038/nature12760.

Rodier, J., and C. Bazin (2005), *Analyse de l'eau: Eaux naturelles, eaux résiduelles et eaux de mer*, 8 éd., Dunod, Paris.

Schopka, H. H., L. A. Derry, and C. A. Arcilla (2011), Chemical weathering, river geochemistry and atmospheric carbon fluxes from volcanic and ultramafic regions on Luzon Island, the Philippines, *Geochim. Cosmochim. Acta*, *75*, 978–1002, doi:10.1016/j.gca.2010.11.014.

Smets, B. (2007), *Etude des mazukus dans la région de Goma (République Démocratique du Congo) et gestion des risques, Mémoire de Master en Gestion des Risques Naturels*, Univ. de Liège, Liège, Belgium.

Smets, B., et al. (2013), Detailed multidisciplinary monitoring reveals pre- and co-eruptive signals at Nyamulagira volcano (North Kivu, Democratic Republic of Congo), *Bull. Volcanol.*, *76*(1), 1–35, doi:10.1007/s00445-013-0787-1.

Spencer, R. G. M., et al. (2012), An initial investigation into the organic matter biogeochemistry of the Congo River, *Geochim. Cosmochim. Acta*, *84*, 614–627, doi:10.1016/j.gca.2012.01.013.

Spitzy, A., and J. Leenheer (1991), dissolved organic carbon in rivers, in *Biogeochemistry of Major World Rivers*, edited by E. T. Degens, S. Kempe, and J. E. Richey, chap. 9, pp. 213–232, John Wiley, N. Y.

Still, C. J., and R. L. Powell (2010), Continental-Scale distributions of vegetation stable carbon isotope ratios, in *Isoscapes: Understanding Movement, Pattern, and Process on Earth Through Isotope Mapping*, edited by J. B. West, et al., pp. 179–193, Springer, Netherlands, doi: 10.1007/978-90-481-3354-3_9.

Tamooh, F. K., et al. (2012), Distribution and origin of suspended matter and organic carbon pools in the Tana River Basin, Kenya, *Biogeosciences*, *9*, 2905–2920, doi:10.5194/bg-9-2905-2012.

Teodoru, C. R., F. C. Nyoni, A. V. Borges, F. Darchambeau, I. Nyambe, and S. Bouillon (2015), Spatial variability and temporal dynamics of greenhouse gas (CO_2, CH_4, N_2O) concentrations and fluxes along the Zambezi River mains tem and major tributaries, *Biogeosciences*, *12*, 2431–2453, doi:10.5194/bg-12-2431-2015.

Vitousek, P. M. (2004), *Nutrient Cycling and Limitation: Hawai'i as a Model System*, Princeton Univ. Press, Princeton, N. J.

Weiss, R. F. (1981), Determinations of carbon dioxide and methane by dual catalyst flame ionization chromatography and nitrous oxide by electron capture chromatography, *J. Chromatogr. Sci.*, *19*, 611–616.

Wieczorek, M. E. (2012), *Flow-Based Method for Stream Generation in a GIS*, USGS Water Sci. Cent. for Md., Delaware and the Dist. of Columbia, USGS. [Available at http://md.water.usgs.gov/posters/flowGIS/index.html.]

Zhang, G. L., J. Zhang, S. M. Liu, J. L. Ren, and Y. C. Zhao (2010), Nitrous oxide in the Changjiang (Yangtze River) Estuary and its adjacent marine area: Riverine input, sediment release and atmospheric fluxes, *Biogeosciences*, *7*, 3505–3516, doi:10.5194/bg-7-3505-2010.